

1 **Response to:**

2 **Comments on “Theoretical investigation of mixing in warm clouds – Part 3:**
3 **Inhomogeneous mixing”**

4

5 **We express our gratitude for valuable comments and remarks.**

6

7 © I have read the revised version of part 3 and in general I think it is ready for publication
8 after some relatively small corrections listed below. As with the revised part 2, there is clearer
9 connection between the three parts and better physical interpretation of the results. In
10 particular, I like the name "potential evaporation parameter" and appreciate the added
11 discussion of its meaning.

12

13 ® Thank you.

14

15 ©1. The title of Fig3c, Fig4c should be $R=-1.5$ not $--1.5$

16 ® Done

17 ©2. page 32, line 734: delete "a" in front of "an"

18 ® Done

19 ©3. page 32, line 740: change "/" to "-"

20 ® Corrected

21 ©4. page 35, line 815: 30-50 not divided

22 ® Corrected

23 ©5. page 35. line 847: add reference to in-situ measurements.

24 ® The reference is added

25

26

27

28

29

30

31

32 **Theoretical analysis of mixing in liquid clouds. Part 3: Inhomogeneous mixing**

33

34 M. Pinsky(1), A. Khain(1), and A. Korolev(2)

35

36 (1) Department of Atmospheric Sciences, The Hebrew University of Jerusalem, Israel

37 (2) Environment Canada, Cloud Physics and Severe Weather Section, Toronto, Canada

38

39

40

Submitted to

41

Atmospheric Chemistry and Physics

42

Revised: April 2016

43

Second revision: May 2016

44

45

46 Communicating author: Alexander Khain, The Hebrew University of Jerusalem,

47 khain@vms.huji.ac.il

48

49

50

51

52

53 **Abstract**

54 An idealized diffusion-evaporation model of time-dependent mixing between a cloud

55 volume and a droplet-free volume is analyzed. The initial droplet size distribution (DSD) in

56 the cloud volume is assumed to be monodisperse. It is shown that evolution of the

57 microphysical variables and the final equilibrium state are unambiguously determined by two

58 non-dimensional parameters. The first one is the potential evaporation parameter R ,

59 proportional to the ratio of the saturation deficit to the liquid water content in the cloud

60 volume, that determines whether the equilibrium state is reached at 100% relative humidity, or
61 is characterized by a complete evaporation of cloud droplets. The second parameter Da is the
62 *Damköhler* number equal to the ratio of the characteristic mixing time to the phase relaxation
63 time. Parameters R and Da determine the type of mixing.

64 The results are analyzed within a wide range of values of R and Da . It is shown that there
65 is no pure homogeneous mixing, since the first mixing stage is always inhomogeneous. The
66 mixing type can change during the mixing process. Any mixing type leads to formation of a tail
67 of small droplets in DSD and, therefore, to DSD broadening that depends on Da . At large Da ,
68 the final DSD dispersion can be as large as 0.2. The total duration of mixing varies from
69 several to one hundred phase relaxation time periods, depending on R and Da .

70 The definitions of homogeneous and inhomogeneous types of mixing are reconsidered and
71 clarified, enabling a more precise delimitation between them. The paper also compares the
72 results obtained with those based on the classic mixing concepts.

73 **Keywords:** homogeneous and inhomogeneous mixing, turbulent diffusion, droplet
74 evaporation

75

76 1. Introduction

77 Cloud physics typically investigates two types of turbulent mixing: homogeneous and
 78 extremely inhomogeneous (e.g. Burner and Brenguier, 2006; Andrejczuk et al., 2009; Devenish
 79 et al., 2012; Kumar et al., 2012). The concept of extremely inhomogeneous mixing in clouds
 80 was introduced by Latham and Reed (1977); Baker and Latham (1979), Baker et al. (1980) and
 81 Blyth et al. (1980). According to this concept, mixing of cloud air and sub-saturated air from
 82 cloud surrounding results in complete evaporation of a fraction of cloud droplets, whereas size
 83 of other droplets remain unchanged. The studies of extremely inhomogeneous mixing were
 84 closely related to investigation of different mechanisms underlying enhanced growth of cloud
 85 droplets and warm precipitation formation (Baker et al., 1980; Baker and Latham, 1982). The
 86 concept of homogeneous mixing suggests that all the droplets partially evaporate, so the liquid
 87 water content decreases while the droplet concentration remains unchanged (Lehmann et al.,
 88 2009; Pt1). The significance of the concepts of homogeneous and inhomogeneous mixing goes
 89 far beyond formation of large-sized droplets. In fact, these concepts are closely related to the
 90 mechanisms involved in formation of droplet size distributions (DSD) in clouds and to the
 91 description of this formation in numerical cloud models. A detailed analysis of the classical
 92 concepts of homogeneous and extremely inhomogeneous mixing is given by Korolev et al.
 93 (2016, hereafter Pt1).

94 Mixing in clouds includes two processes: mechanical mixing caused by turbulent diffusion
 95 and droplet evaporation accompanied by increasing relative humidity. The relative contribution
 96 of these processes can be evaluated by comparison of two characteristic time scales: the
 97 characteristic mixing time scale $\tau_{mix} \sim L^{2/3} \varepsilon^{-1/3}$ (where L is the characteristic linear scale of an
 98 entrained volume and ε is the dissipation rate of turbulent kinetic energy) and the time of
 99 phase relaxation $\tau_{pr} = (4\pi \mathcal{D} \bar{r} N)^{-1}$ (where N is droplet concentration in a cloud volume, \bar{r} is
 100 the mean droplet radius and \mathcal{D} is the diffusivity of water vapor) characterizing the response of
 101 the droplet population to changes in humidity (the list of notations is given in Appendix). The

102 choice of the phase relaxation time as the characteristic time scale of mixing is discussed by
103 Pinsky et al. (2016) (hereafter referred to as Pt. 2) and will be further elaborated below.

104 Mixing is considered homogeneous if $\tau_{mix} / \tau_{pr} \ll 1$. At the first stage of mixing, the initial
105 gradients of the microphysical and thermodynamic variables rapidly decrease to zero. By the
106 end of this stage, the fields of temperature, humidity (hence, the relative humidity, RH) and
107 droplet concentration are spatially homogenized and all the droplets within the mixing volume
108 experience the same saturation deficit. During the relatively lengthy second stage, droplets
109 evaporate and increase the relative humidity in the volume. It was shown that homogeneous
110 mixing takes place at scales below about 0.5 m (Pt. 2)

111 At spatial scales larger than ~ 0.5 m, $\tau_{mix} / \tau_{pr} > 1$ and the spatial gradients of RH remain for
112 a long time. Consequently, droplets within the mixing volume experience different
113 subsaturations, thus the mixing is considered inhomogeneous. At $\tau_{mix} / \tau_{pr} \gg 1$, the mixing is
114 considered extremely inhomogeneous.

115 According to the classical conceptual scheme, during the first stage of extremely
116 inhomogeneous mixing a fraction of droplets is transported into the droplet-free entrained
117 volume and evaporates completely. The evaporation continues until the evaporating droplets
118 saturate the initially droplet-free volume. At the second stage, turbulent mixing between the
119 cloud volume and the initially droplet-free (but already saturated) volume homogenizes the
120 gradients of droplet concentration and other quantities. Since both volumes are saturated,
121 mixing does not affect droplet sizes. As a result, the final (equilibrium) state is characterized by
122 the relative humidity RH=100% and the DSD shape similar to that before mixing, but with a
123 lower droplet concentration. The same result (a decrease in droplet concentration but
124 unchanged droplet size) is expected in cases of both monodisperse and polydisperse initial
125 DSD. Since the DSD shape does not change, the characteristic droplet sizes (i.e. the mean

126 square radius, the mean volume radius and the effective radius) do not change either in the
127 course of extremely inhomogeneous mixing.

128 Thus, according to the classical concepts, the final equilibrium state with RH=100% is
129 reached either by a partial evaporation of all droplets (homogeneous mixing) or a total
130 evaporation of a certain portion of droplets that does not affect the remaining droplets
131 (extremely inhomogeneous mixing) (Lehmann et al., 2009; Pt1).

132 In analyses of in-situ measurements, the observed data are usually compared with those
133 expected at the final state of mixing as assumed by the classical mixing concepts. If droplet
134 concentration decreases without a corresponding change in the characteristic droplet radius,
135 the mixing is considered “extremely inhomogeneous.” If the characteristic droplet radius
136 decreases with an increase of the dilution level while droplet concentration decreases
137 insignificantly, the mixing is identified as “homogeneous.” If both the characteristic droplet
138 radius and the droplet concentration change, the mixing is considered as "intermediate".
139 Quantitative evaluations of the microphysical processes specific for intermediate mixing
140 remain largely uncertain.

141 As was discussed in Pt 2, the final states of mixing suggested by the classical concepts are
142 only hypothetical. To understand the essence of the final equilibrium states of mixing and
143 evaluate the time needed to reach them, it is necessary to consider the time evolution of DSD in
144 the course of mixing process. Time-dependent process of homogeneous mixing was analyzed
145 in Pt. 2. It was shown that in important cases of wide polydisperse initial DSDs, the final state
146 substantially differs from that hypothesized by the classical concepts.

147 In this study, which is a Pt 3 of the set of studies, we analyze the time-dependent process of
148 inhomogeneous mixing. The structure of the paper is as follows. The main concept and the
149 basic equations for time-dependent inhomogeneous mixing are described in Section 2. Analysis
150 of non-dimensional diffusion-evaporation equations is presented in Section 3. The design and
151 the results of simulations of non-homogeneous mixing are outlined in Sections 4 and 5. A

152 discussion clarifying the concepts of homogeneous and inhomogeneous mixing is presented in
 153 concluding Section 6.

154

155 **2. The main concept and the basic equations**

156 During mixing of cloud volume and entrained air volume, the following two processes
 157 determine the change of the microphysical and thermodynamical variables: turbulent diffusion
 158 resulting in mechanical smoothening of the gradients of temperature, water vapor and droplet
 159 concentration, and droplet evaporation accompanied by phase transformation. In this study,
 160 inhomogeneous mixing is investigated based on the analysis and solution of a 1D diffusion-
 161 evaporation equation. To our knowledge, the idea of using a diffusive model of turbulent
 162 mixing to describe the mixing process was first proposed by Baker and Latham (1982). A
 163 diffusion-evaporation equation was also analyzed by Jeffery and Reisner (2006). In order to get
 164 a more precise understanding of the physics of mixing process the analysis is performed under
 165 the following main simplifying assumptions:

- 166 a) turbulent mixing is analyzed neglecting vertical motions of mixing volumes, droplet
 167 collisions and droplet sedimentation.
- 168 b) the total mixing volume is assumed adiabatic.
- 169 c) mixing is assumed to take place only along the x -direction, i.e. a 1D task is considered;
- 170 d) the initial DSD in the cloud volume is assumed monodisperse.

171 Other assumptions and simplifications are discussed below.

172

173 A schematic illustration of the initial conditions used in the study is shown in **Figure 1**.
 174 Two air volumes are assumed to mix: a cloud volume (left) and a droplet-free volume (right),
 175 each having the linear size of $L/2$. The value of L is assumed within the range of several tens
 176 to a few hundred meters. The mixing starts at $t = 0$. The cloud volume is initially saturated
 177 $S_1 = 0$, the initial droplet concentration is N_1 and the initial liquid water mixing ratio is

178 $q_1 = \frac{4\pi\rho_w}{3\rho_a} N_1 r_0^3$. In the droplet-free volume the initial conditions are $RH_2 < 100\%$ (i.e.
 179 $S_2 < 0$), $N_2 = 0$ and $q_2 = 0$. Therefore, the initial profiles of these quantities along the x -axis
 180 are step functions

$$181 \quad N(x,0) = \begin{cases} N_1 & \text{if } 0 \leq x < L/2 \\ 0 & \text{if } L/2 \leq x < L \end{cases} \quad (1a)$$

$$182 \quad S(x,0) = \begin{cases} 0 & \text{if } 0 \leq x < L/2 \\ S_2 & \text{if } L/2 \leq x < L \end{cases} \quad (1b)$$

$$183 \quad q(x,0) = \begin{cases} q_1 & \text{if } 0 \leq x < L/2 \\ 0 & \text{if } L/2 \leq x < L \end{cases} \quad (1c)$$

184 The initial profile of droplet concentration is shown in Fig. 1. In this study, averaged equations
 185 are used. We do not consider mixing at scales below several millimeters. At the scales of
 186 averaging, there exist clear definitions of droplet concentration, supersaturation and other "macro
 187 scale" quantities. The mixing is assumed to be driven by isotropic turbulence within the inertial
 188 sub-range where the Richardson's law is valid. Accordingly, turbulent diffusion (turbulent
 189 mixing) is described by a 1D equation of turbulent diffusion with a turbulent coefficient K . The
 190 turbulent coefficient is evaluated as proposed by Monin and Yaglom (1975)

191

$$192 \quad K(L) = C\varepsilon^{1/3}L^{4/3} \quad (2)$$

193 In Eq. (2), C is a constant. Eq. (2) is valid in case turbulent diffusion is considered, i.e. at scales
 194 where molecular diffusion can be neglected.

195 Since the total mixing volume is adiabatic, the fluxes of different quantities through the left
 196 and right boundaries of the volume are equal to zero at any time instance, i.e.

$$197 \quad \frac{\partial N(0,t)}{\partial x} = \frac{\partial N(L,t)}{\partial x} = 0; \quad \frac{\partial q(0,t)}{\partial x} = \frac{\partial q(L,t)}{\partial x} = 0; \quad \frac{\partial q_v(0,t)}{\partial x} = \frac{\partial q_v(L,t)}{\partial x} = 0 \quad (3)$$

198 where q_v is the water vapor mixing ratio.

199 During mixing, droplets in the mixing volume experience different subsaturations,
 200 therefore, the initially monodisperse DSD will become polydisperse. The droplets that were

201 transported into the initially droplet-free volume will undergo either partial or complete
 202 evaporation. The evaporation leads to a decrease in both droplet size and droplet concentration.

203 The basic system of equations that describes the processes of diffusion and of evaporation
 204 which occur simultaneously is to be derived. The first equation is written for value Γ defined
 205 as

$$206 \quad \Gamma = S + A_2 q \quad (4)$$

207 This value is conservative in a moist adiabatic process, i.e. it does not change during phase
 208 transitions (Pinsky et al., 2013, 2014). In Eq. (4), the coefficient $A_2 = \frac{1}{q_v} + \frac{L_w^2}{c_p R_v T^2}$ is a weak

209 function of temperature that changes by $\sim 10\%$ when temperatures change by $\sim 10^\circ\text{C}$ (Pinsky et
 210 al., 2013). In this study, it is assumed that $A_2 = \text{constant}$. In Eq. (4), $q = \frac{4\pi\rho_w}{3\rho_a} \int_0^\infty r^3 f(r) dr$ is the

211 liquid water mixing ratio and $f(r)$ is the DSD. The quantity Γ obeys the diffusion equation

$$212 \quad \frac{\partial\Gamma(x,t)}{\partial t} = K \frac{\partial^2\Gamma(x,t)}{\partial x^2} \quad (5)$$

213 with the boundary conditions $\frac{\partial\Gamma(0,t)}{\partial x} = \frac{\partial\Gamma(L,t)}{\partial x} = 0$ and the initial profile at $t = 0$

$$214 \quad \Gamma(x,0) = \begin{cases} A_2 q_1 & \text{if } 0 \leq x < L/2 \\ S_2 & \text{if } L/2 \leq x < L \end{cases} \quad (6)$$

215 Therefore, function $\Gamma(x,0)$ is positive in the left volume, and negative in the right volume.

216 Since Γ does not depend on phase transitions, Eq. (5) can be solved independently of other
 217 equations. The solution of Eq. (5) with initial conditions (6) is (Polyanin and Zaitsev, 2004)

$$218 \quad \Gamma(x,t) = \sum_{n=0}^{\infty} a_n \exp\left(-\frac{Kn^2\pi^2 t}{L^2}\right) \cos\left(\frac{n\pi x}{L}\right) = \quad (7)$$

$$\frac{1}{2}(S_2 + A_2 q_1) + (A_2 q_1 - S_2) \sum_{n=1}^{\infty} \frac{\sin(n\pi/2)}{n\pi/2} \exp\left(-\frac{Kn^2\pi^2 t}{L^2}\right) \cos\left(\frac{n\pi x}{L}\right)$$

219 where the Fourier coefficients of expanding the step function (6) are

$$220 \quad a_0 = \frac{1}{2}(A_2 q_1 + S_2) \quad (8a)$$

$$221 \quad a_n = (A_2 q_1 - S_2) \frac{\sin(n\pi/2)}{n\pi/2}, \quad n = 1, 2, \dots \quad (8b)$$

222 An example of spatial dependencies of $\Gamma(x, t)$ at different time instances during the mixing is
 223 shown in **Figure 2**. One can see a decrease in the initial gradients and a tendency to
 224 establishing a horizontally uniform value of Γ . Since the initial volume was divided into two
 225 equal parts, the diffusion leads to formation of a constant limit value of function Γ

$$226 \quad \Gamma(x, \infty) = \frac{1}{2}(\Gamma(0, 0) + \Gamma(L, 0)).$$

227 The second basic equation is the equation for diffusional droplet growth, taken in the
 228 following form (Pruppacher and Klett, 2007)

$$229 \quad \frac{d\sigma}{dt} = \frac{2S}{F} \quad (9)$$

230 where $\sigma = r^2$ is the square of droplet radius and $F = \frac{\rho_w L_w^2}{k_a R_v T^2} + \frac{\rho_w R_v T}{e_s(T) \mathcal{D}}$. The value of

231 coefficient F is considered constant in this study. The solution of Eq. (9) is

$$232 \quad \sigma(t) = \frac{2}{F} \int_0^t S(t') dt' + \sigma_0 \quad (10)$$

233 The third main equation describes the evolution of DSD. In the following discussion, the
 234 DSD will be presented in the form $g(\sigma)$ which is the distribution of the square of the radius.
 235 This formulation directly utilizes the property of the diffusion growth equation (9) according to
 236 which the time changes of DSD are reduced to shifting the distributions in the space of square
 237 radii, while the shape of the distribution remains unchanged. The standard DSD $f(r)$ is related
 238 to $g(\sigma)$ as $f(r) = 2r \cdot g(r^2)$.

239 The normalized condition for $g(\sigma)$ is

$$240 \quad N = \int_0^{\infty} g(\sigma) d\sigma \quad (11)$$

241 where N is the droplet concentration. Using DSD $g(\sigma)$, the liquid water mixing ratio can be
 242 presented as integral

$$243 \quad q = \frac{4\pi\rho_w}{3\rho_a} \int_0^{\infty} \sigma^{3/2} g(\sigma) d\sigma \quad (12)$$

244 The 1D diffusion-evaporation equation for the non-conservative function $g(\sigma)$ can be
 245 written in the form (Rogers and Yau, 1989)

$$246 \quad \frac{\partial g(\sigma)}{\partial t} = K \frac{\partial^2 g(\sigma)}{\partial x^2} - \frac{\partial}{\partial \sigma} \left(\frac{d\sigma}{dt} g(\sigma) \right) \quad (13)$$

247 where the first term on the right-hand side of Eq. (13) describes changes in the DSD due to
 248 spatial diffusion, while the second term on the right-hand side describes changes in the DSD
 249 due to evaporation. Substitution of Eq. (9) into Eq. (13) leads to the following equation

$$250 \quad \frac{\partial g(x,t,\sigma)}{\partial t} = K \frac{\partial^2 g(x,t,\sigma)}{\partial x^2} - \frac{2S(x,t)}{F} \frac{\partial g(x,t,\sigma)}{\partial \sigma} \quad (14)$$

251 To close Eq. (14), Eq. (4) should be used in the form

$$252 \quad S(x,t) = \Gamma(x,t) - A_2 q(x,t) \quad (15)$$

253 where $q(x,t)$ is calculated according to Eq. (12). Eqs. (12, 14, 15) constitute a closed set of
 254 equations allowing calculation of $g(x,t,\sigma)$.

255 To proceed to the equations for DSD moments, let us define a moment of DSD $g(\sigma)$ of
 256 order α as

$$257 \quad m_\alpha = \overline{\sigma^\alpha} = \int_0^{\infty} \sigma^\alpha g(\sigma) d\sigma \quad (16)$$

258 Multiplying Eq. (14) by σ^α , integrating within limits $[0..\infty]$ and assuming that $\sigma^\alpha g(\sigma) \rightarrow 0$
 259 when $\sigma \rightarrow \infty$, yield a recurrent formula for the DSD moments

260

$$261 \quad \frac{\partial m_\alpha(x,t)}{\partial t} = K \frac{\partial^2 m_\alpha(x,t)}{\partial x^2} + \alpha \frac{2S}{F} m_{\alpha-1}(x,t) \quad (17)$$

262 Eq. (17) provides a recurrent relationship between the DSD moments of different orders. This
 263 relationship was discussed by Pinsky et al.'s (2014) while analyzing diffusion growth in an
 264 ascending adiabatic parcel.

265 In particular, the equation for the liquid water mixing ratio that is a moment of the order of
 266 $\alpha = \frac{3}{2}$ can be written as

$$267 \quad \frac{\partial q(x,t)}{\partial t} = K \frac{\partial^2 q(x,t)}{\partial x^2} + \frac{4\pi\rho_w N(x,t)\bar{r}(x,t)}{F\rho_a} S(x,t) \quad (18)$$

268 where the mean radius $\bar{r}(x,t) = \frac{m_{1/2}}{m_0}$.

269 In the general case, Eq. (18) is not closed, since concentration $N(x,t)$ and $\bar{r}(x,t)$ are unknown
 270 functions of time and spatial coordinates.

271 The characteristic time of evaporation and of supersaturation change is the phase relaxation
 272 time (Korolev and Mazin, 2003)

$$273 \quad \tau_{pr} = \frac{\rho_a F}{4\pi\rho_w A_2 N \bar{r}} \quad (19)$$

274 Using Eq. (19), Eq. (18) can be rewritten as

$$275 \quad \begin{aligned} \frac{\partial q(x,t)}{\partial t} &= K \frac{\partial^2 q(x,t)}{\partial x^2} + \frac{1}{\tau_{pr}(x,t)} \left[\frac{1}{A_2} \Gamma(x,t) - q(x,t) \right] = \\ &= K \frac{\partial^2 q(x,t)}{\partial x^2} + \frac{1}{A_2 \tau_{pr}(x,t)} S(x,t) \end{aligned} \quad (20)$$

276 From Eqs. (20) and (15), the equation for supersaturation can be written in the following simple
 277 form

$$278 \quad \frac{\partial S(x,t)}{\partial t} = K \frac{\partial^2 S(x,t)}{\partial x^2} - \frac{S(x,t)}{\tau_{pr}(x,t)} \quad (20a)$$

279 Eqs. (20) and (20a) show that changes in the microphysical variables are determined by the rate
 280 of spatial diffusion (the first term on the right-hand side of these equations) and of evaporation
 281 (the second term on the right-hand side).

282

283 **3. Analysis of non-dimensional equations**

284 Spatial diffusion and evaporation depend on many parameters. It is the best to start the
 285 analysis from the basic equation system presented in a non-dimensional form. A time scale
 286 corresponding to the initial phase relaxation time in a cloud volume can be defined as

$$287 \quad \tau_0 = \frac{\rho_a F}{4\pi\rho_w A_2 N_1 r_0} \quad (21)$$

288 and the non-dimensional time is $\tilde{t} = t / \tau_0$. Other non-dimensional parameters to be used are:

289 the non-dimensional phase relaxation time

$$290 \quad \tilde{\tau}_{pr} = \tau_{pr} / \tau_0 = \frac{N_1 r_0}{N(\tilde{x}, \tilde{t}) \bar{F}(\tilde{x}, \tilde{t})}, \quad (22a),$$

291 the normalized liquid water mixing ratio which is equal to the normalized liquid water content

$$292 \quad \tilde{q} = \frac{q}{q_1}, \quad (22b),$$

293 the normalized supersaturation

$$294 \quad \tilde{S} = \frac{S}{A_2 q_1} \quad (22c),$$

295 the non-dimensional conservative function

$$296 \quad \tilde{\Gamma} = \frac{\Gamma}{A_2 q_1}, \quad (22d),$$

297 the normalized square of droplet radius

$$298 \quad \tilde{\sigma} = \frac{\sigma}{r_0^2}, \quad (22e),$$

299 the normalized droplet concentration

$$300 \quad \tilde{N} = N / N_1 \quad (22f)$$

301 and the non-dimensional DSD

$$302 \quad \tilde{g}(\tilde{\sigma}) = \frac{r_0^2}{N_1} g(\sigma) \quad (22g).$$

303 with normalization $\tilde{N} = \int_0^1 \tilde{g}(\tilde{\sigma}) d\tilde{\sigma}$. The definition (22g) means that the integral of a non-
304 dimensional initial size distribution over the normalized square radius is equal to unity.

305 The non-dimensional distance and the non-dimensional time are defined as

$$306 \quad \tilde{x} = x/L; \quad \tilde{t} = t/\tau_0 \quad (22h)$$

307 A widely used non-dimensional parameter showing the comparative rates of diffusion and
308 evaporation is the Damkölher number:

$$309 \quad Da = \frac{\tau_{mix}}{\tau_0} = \frac{L^2}{K\tau_0} \quad (23)$$

310 where

$$311 \quad \tau_{mix} = \frac{L^2}{K} \quad (24)$$

312 is the characteristic time scale of mixing. Using the non-dimensional parameters listed above,
313 Eq. (20) can be rewritten in a non-dimensional form as

314

$$315 \quad \frac{\partial \tilde{q}(\tilde{x}, \tilde{t})}{\partial \tilde{t}} = \frac{1}{Da} \frac{\partial^2 \tilde{q}(\tilde{x}, \tilde{t})}{\partial \tilde{x}^2} + \frac{1}{\tilde{\tau}_{pr}(\tilde{x}, \tilde{t})} [\tilde{\Gamma}(\tilde{x}, \tilde{t}) - \tilde{q}(\tilde{x}, \tilde{t})] =$$

$$\frac{1}{Da} \frac{\partial^2 \tilde{q}(\tilde{x}, \tilde{t})}{\partial \tilde{x}^2} + \frac{1}{\tilde{\tau}_{pr}(\tilde{x}, \tilde{t})} \tilde{S}(\tilde{x}, \tilde{t}) \quad (25)$$

316 where

$$317 \quad \tilde{q}(\tilde{x}, \tilde{t}) = \frac{N(\tilde{x}, \tilde{t}) \overline{\sigma^{3/2}}}{N_1 r_0^3} = \int_0^\infty \tilde{\sigma}^{3/2} \tilde{g}(\tilde{x}, \tilde{t}, \tilde{\sigma}) d\tilde{\sigma} \quad (26)$$

318 The initial conditions and the boundary conditions should be rewritten in a non-dimensional
319 form as well. For instance, the normalized initial condition for the non-dimensional function
320 $\tilde{q}(\tilde{x}, 0)$ can be derived from Eqs. (1c) and (22b)

$$321 \quad \tilde{q}(\tilde{x}, 0) = \begin{cases} 1 & \text{if } 0 \leq \tilde{x} < 1/2 \\ 0 & \text{if } 1/2 \leq \tilde{x} < 1 \end{cases} \quad (27)$$

322 The solution for $\tilde{\Gamma}(\tilde{x}, \tilde{t})$ obtained by a normalization of solution (7) is

$$323 \quad \tilde{\Gamma}(\tilde{x}, \tilde{t}) = \frac{1}{2}(1+R) + (1-R) \sum_{n=1}^{\infty} \frac{\sin(n\pi/2)}{n\pi/2} \exp\left(-\frac{n^2\pi^2\tilde{t}}{Da}\right) \cos(n\pi\tilde{x}), \quad (28)$$

324 where

$$325 \quad R = \frac{S_2}{A_2 q_1} \quad (29)$$

326 is a non-dimensional parameter referred to, hereafter, as a potential evaporation parameter
 327 (PEP). The PEP is proportional to the ratio of the amount of water vapour that should
 328 evaporate in order to saturate the initially droplet-free volume (that is determined by S_2) to the
 329 initial available liquid water q_1 in the cloud volume. The solution of Eq. (28) at $t \rightarrow \infty$ depends
 330 only on parameter R .

$$331 \quad \tilde{\Gamma}(\tilde{x}, \infty) = \frac{1}{2}(1+R) \quad (30)$$

332 The importance of PEP that determines a possible final state was illustrated in Pt. 1. PEP is
 333 also the sole parameter enabling calculation of the normalized mixing diagram for
 334 homogeneous mixing (Pt. 2). In this study, we consider cases when $R < 0$ since $S_2 < 0$, i.e.
 335 when droplets can only evaporate in the course of mixing.

336 The solution of Eq. (25) and the type of mixing depends on the values of two non-
 337 dimensional parameters, namely, Da and R . Thus, when $R = \frac{S_2}{A_2 q_1} < -1$, $\tilde{\Gamma}(\tilde{x}, \infty) < 0$. It means
 338 that the initially droplet-free volume V_2 is too dry and all the droplets in the mixing volume
 339 evaporate completely. At the final equilibrium state $RH < 100\%$, i.e. $S(x, \infty) < 0$. If

340 $R = \frac{S_2}{A_2 q_1} > -1$, $\tilde{\Gamma}(\tilde{x}, \infty) > 0$. This means that the mixed volume in the final state contains

341 droplets, i.e. the mixing leads expands the volume with droplets, i.e. the cloud volume. At the

342 final equilibrium state, $RH = 100\%$ (i.e. $S(x, \infty) = 0$). The case when $|R| = \left| \frac{S_2}{A_2 q_1} \right| = |\tilde{S}_2| \ll 1$
 343 corresponds to either RH close to 100% (i.e. S_2 is close to zero) (this case corresponds to the
 344 degenerated case considered in Pt. 1), and/or to the case when the liquid water mixing ratio in
 345 the cloud volume is large. In case $|R| \ll 1$, the second term on the right-hand side of Eq. (25) is
 346 much smaller than the first term, and the mixing is driven by turbulent diffusion only.

347 In case $Da \rightarrow 0$ (often considered as homogeneous mixing), at the beginning of the mixing
 348 the diffusion term is much larger than the evaporation term, the second term on the right-hand
 349 side of Eq. (25). As mixing proceeds, within a short time period the total homogenization of all
 350 the variables in the mixing volume is established and all the spatial gradients become equal to
 351 zero. At this time instance, the first term on the right-hand side becomes equal to zero, and the
 352 second term on the right-hand side of Eq. (25), describing droplet evaporation, becomes
 353 dominant. Thus, the analysis of the Eq. (25) shows that mixing consists of two stages. The first
 354 mixing stage is a short stage of inhomogeneous mixing and the longer second stage of
 355 homogeneous mixing. The evolution of the microphysical variables during homogeneous
 356 mixing is described in detail in Pt. 2.

357 $Da \rightarrow \infty$ corresponds to extremely inhomogeneous mixing, according to the classic
 358 concept. In this case, the diffusion term is much smaller than the evaporation term, so
 359 evaporation takes place under significant spatial gradients of RH . At $Da = \infty$, the adjacent
 360 volumes do not mix at all and remain separated. This equivalent to existence of two
 361 independent adiabatic volumes. Another interpretation of the limiting case $Da = \infty$ is an
 362 infinite fast droplet evaporation. Both scenarios at $Da \rightarrow \infty$ indicate simplifications in the
 363 definition of the extremely inhomogeneous mixing. At intermediate values of Da , mixing is
 364 inhomogeneous, when both turbulent diffusion and evaporation contribute simultaneously to
 365 formation of the DSD.

366 Using Eq. (14) and normalization (22f), the equations for the non-dimensional size
 367 distribution can be written as

$$368 \quad \frac{\partial \tilde{g}(\tilde{x}, \tilde{t}, \tilde{\sigma})}{\partial \tilde{t}} = \frac{1}{Da} \frac{\partial^2 \tilde{g}(\tilde{x}, \tilde{t}, \tilde{\sigma})}{\partial \tilde{x}^2} + \frac{2}{3} [\tilde{\Gamma}(\tilde{x}, \tilde{t}) - \tilde{q}(\tilde{x}, \tilde{t})] \frac{\partial \tilde{g}(\tilde{x}, \tilde{t}, \tilde{\sigma})}{\partial \tilde{\sigma}} \quad (31)$$

369

370 Eq. (31) is solved with the following initial conditions

371

$$372 \quad \tilde{g}(\tilde{x}, 0, \tilde{\sigma}) = \begin{cases} \delta(\tilde{\sigma} - 1) & \text{if } 0 \leq \tilde{x} < 1/2 \\ 0 & \text{if } 1/2 \leq \tilde{x} \leq 1 \end{cases} \quad (32)$$

373 where $\delta(\tilde{\sigma} - 1)$ is a delta function.

374

375 **Table 1** presents the list of all the non-dimensional variables used in this study and the
 376 ranges of their variation. It is shown that six parameters determining the geometrical and
 377 microphysical properties of mixing can be reduced to two non-dimensional parameters, which
 378 enables a more efficient analysis of mixing. The ranges of parameter variations in Tab. 1
 379 correspond to the simplifications used in the study (the initial DSD is monodisperse
 380 and $RH \leq 100\%$).

381

382 **4. Design of simulations**

383 ***Damköhler number Da in clouds***

384 The characteristic mixing time τ_{mix} can be evaluated using Eqs. (2) and (24)

$$385 \quad \tau_{mix} = \frac{1}{C} \varepsilon^{-1/3} L^{2/3} \quad (33)$$

386 There is significant uncertainty regarding the evaluation of τ_{mix} and Da in clouds, which is
 387 largely related to the choice of coefficient C in expression (33). These values differ in different
 388 studies: $C = 10$ (Jeffery and Reisner, 2006); $C = 1$ (Lehmann et al., 2009) and $C \approx 0.2$ (
 389 Monin and Yaglom, 1975) and Boffetta and Sokolov (2002).

390 According to Lehmann et al. (2009), the values of Da in clouds of different types range
 391 from to 0.1 to several hundred. Thus, estimation of Da in clouds may vary within a wide range
 392 up to a few orders of magnitude. Da values of in stratocumulus clouds can be similar or even
 393 higher than those in cumulus clouds, since both τ_{mix} and τ_{pr} in stratiform clouds are larger than
 394 in cumulus clouds.

395 In our simulations, we compare the evolution of the microphysical parameters within a
 396 wide range of Da (from 1 up to 500) and of R (from -1.5 up to -0.1). $Da = 1$ represents the
 397 case closest to homogeneous mixing, while $Da = 500$ indicates extremely inhomogeneous
 398 mixing.

399

400 ***Numerical method***

401 Calculations were performed using MATLAB solver PDEPE. We solve the equation
 402 system (31) for normalized DSD $\tilde{g}(\tilde{x}, \tilde{t}, \tilde{\sigma}_j)$ with the initial condition (32) and the Neumann
 403 boundary conditions

404

$$405 \quad \frac{\partial \tilde{g}(0, \tilde{t}, \tilde{\sigma}_j)}{\partial \tilde{x}} = \frac{\partial \tilde{g}(1, \tilde{t}, \tilde{\sigma}_j)}{\partial \tilde{x}} = 0 \quad (34)$$

406 where $j = 1 \dots 24$ are the bin numbers on a linear grid of square radii. The number of grid points
 407 along the \tilde{x} axis was set equal to 81.

408 In calculation of the last term on the right-hand side of Eq. (31), the normalized
 409 supersaturation \tilde{S} was calculated first using the normalized conservative equation

$$410 \quad \tilde{S}(\tilde{x}, \tilde{t}) = \tilde{\Gamma}(\tilde{x}, \tilde{t}) - \tilde{q}(\tilde{x}, \tilde{t}) \quad (35)$$

411 where $\tilde{\Gamma}(\tilde{x}, \tilde{t})$ is calculated using Eq. (28). Then, this term was formulated using Eq. (9) as

$$412 \quad \frac{2}{3} \tilde{S}(\tilde{x}, \tilde{t}) \frac{\partial \tilde{g}(\tilde{x}, \tilde{t}, \tilde{\sigma}_j)}{\partial \tilde{\sigma}_j} \approx \frac{\tilde{g}\left(\tilde{x}, \tilde{t}, \tilde{\sigma}_j + \frac{2}{3} \tilde{S} \Delta \tilde{t}\right) - \tilde{g}(\tilde{x}, \tilde{t}, \tilde{\sigma}_j)}{\Delta \tilde{t}} \quad (36)$$

413 Therefore, at each time step, the DSD \tilde{g} first was shifted to the left to the value $\frac{2}{3}\tilde{S}\Delta\tilde{t}$, where
 414 $\Delta\tilde{t}$ is a small time increment chosen so that $\left|\frac{2}{3}\tilde{S}_{\max}\Delta\tilde{t}\right| \leq \frac{\Delta\tilde{\sigma}}{2}$. Next, the shifted DSD was
 415 remapped onto the fixed square radius grid $\tilde{\sigma}_j$. We used the remapping method proposed by
 416 Kovetz and Olund (1969), which conserves droplet concentration and LWC. After remapping,
 417 the differences between the new and old DSDs were recalculated. The new values of LWC then
 418 were determined using new values of DSD and Eq. (26). MATLAB utility PDEPE
 419 automatically chooses the time step needed to provide stability of calculations.

420

421 **5. Results of simulations**

422 **5.1 Full evaporation case**

423 First, we consider the case $R = -1.5$, when all the cloud water evaporates completely. This
 424 process corresponds to the cloud dissipation caused by mixing with the entrained dry air. At the
 425 final state, RH is expected to be uniform and negative over the entire mixing volume.

426 **Figure 3** shows spatial and time changes of \tilde{S} for $Da = 1, 50$ and 500 . At the final state
 427 for all the three cases $\tilde{S} = -0.25$, which is in agreement with the analytical solution of Eq. (30).
 428 The final negative value indicates that all the droplets completely evaporated during mixing. At
 429 $Da = 1$ (Fig.3ab), two stages of supersaturation evolution can be identified. The first short
 430 stage with $t < 0.4\tau_{pr}$ is the period of inhomogeneous mixing, when the gradients of RH
 431 persist. By end of the second stage of about $14\tau_{pr}$, the equilibrium state is reached. Thus, at
 432 small Da both types of mixing take place. In the cases of $Da = 50$ and $Da = 500$, the spatial
 433 gradients exit during the entire period of mixing until the equilibrium state is reached
 434 (approximately $50\tau_{pr}$ and $300\tau_{pr}$, respectively) (Fig.3cdef). Therefore, at these Da mixing is
 435 inhomogeneous during entire mixing.

436 **Figure 4** shows spatial changes (upper row) and changes in $\tilde{x}-\tilde{t}$ coordinates (lower row)
 437 of normalized LWC for the same case as in Fig.3. These diagrams demonstrate a significant
 438 difference in the evaporation rates at different Da values. Complete evaporation (LWC=0) is
 439 reached at $Da = 1, 50$ and 500 by about 12, 22 and 120 relaxation times periods , respectively.

440 Analysis of Figs. 3 and 4 allows to introduce two characteristic time periods: (1) period T_{mix}
 441 during which the spatial gradients of the microphysical parameters persist, and mixing is
 442 inhomogeneous, and (2) period T_{ev} during which droplet evaporation takes place. Both time
 443 periods are dimensionless and normalized using τ_0 . Time period T_{ev} is equal either to the time
 444 of complete droplet evaporation (when $R < -1.0$) or to the time period during which the
 445 saturation deficit in the mixing volume becomes equal to zero (or close to zero if $R > -1.0$),
 446 i.e. evaporation is actually terminated. Quantitative evaluations of T_{mix} and T_{ev} will be given in
 447 Section 5.3. At $\tilde{t} < T_{mix}$, droplets in the mixing volume experience different saturation deficits.
 448 Toward the end of time T_{mix} the saturation deficit becomes uniform over the entire mixing
 449 volume because of mechanic mixing. At $Da = 1$, the homogenization of the saturation deficit
 450 and all the microphysical variables takes place during a very short time of about $0.5\tau_{pr}$, and
 451 then the evaporation of droplets is assumed to take place under the same subsaturation
 452 conditions, so $T_{mix} \ll T_{ev}$.

453 Figs. 4a,b show that at $\tilde{t} \approx 0.35$, normalized LWC drops down from 1 to 0.4. Since the
 454 average value of the normalized LWC in the mixing volume is equal to 0.5 (see the initial
 455 condition in Eq. (27)), 20% of the droplet mass evaporates during this short inhomogeneous
 456 period. Thus, despite being quite short, inhomogeneous mixing stage plays an important role
 457 even at $Da = 1$.

458 Since at $t = 0$ the mixing volume is not spatially homogeneous by definition, there is
 459 always a period while spatial inhomogeneity exists. With increasing Da , the duration of the
 460 inhomogeneous stage increases and the duration of the homogeneous stage decreases. At

461 $Da = 500$, homogenization of the saturation deficit requires $250\tau_{pr}$, which is twice as long as
 462 the time of complete droplet evaporation, i.e. $T_{mix} \approx 2T_{ev}$. This means that at $Da = 500$, droplet
 463 evaporation takes place in the presence of the spatial gradients of supersaturation. After
 464 complete evaporation of droplets, spatial gradients of the water vapour mixing ratios remain.
 465 This kind of mixing is regarded as inhomogeneous.

466 At $Da = 50$, the time of complete evaporation is approximately equal to the time of
 467 supersaturation homogenization, i.e. $T_{mix} \approx T_{ev}$. In this case, as at $Da = 500$, the droplets
 468 experience different saturation deficit within the mixing volume, so mixing is inhomogeneous
 469 at $Da = 50$.

470 The differences in droplet evaporation at different Da can be seen in **Figure 5.**, showing
 471 the relationships between \tilde{N} and \tilde{q} plotted with a certain time increment, so that each symbol
 472 in the diagrams corresponds to a particular time instance. These symbols form curves. Each
 473 panel of Fig. 5 shows three curves corresponding to different \tilde{x} : the centre of the initially cloud
 474 volume ($\tilde{x} = 1/4$); the centre of the mixing volume ($\tilde{x} = 1/2$) and the centre of the initially
 475 droplet-free volume ($\tilde{x} = 3/4$). The directions of the time increase are shown by arrows along
 476 the corresponding curves. The initial points of the curves corresponding to $\tilde{t} = 0$ are
 477 characterized by values $\tilde{q} = 1$ and $\tilde{N} = 1$ at $\tilde{x} = 1/4$, and by values $\tilde{q} = 0$ and $\tilde{N} = 0$ at $\tilde{x} = 3/4$.

478 The behaviour of the $\tilde{N} - \tilde{q}$ relationship provides important information about mixing
 479 process. At $\tilde{t} < T_{mix}$, there are spatial gradients of \tilde{N} and \tilde{q} , i.e. \tilde{N} and \tilde{q} are different at
 480 different \tilde{x} . This means that the three curves at $\tilde{t} < T_{mix}$ do not coincide. At $\tilde{t} > T_{mix}$, the spatial
 481 gradients of \tilde{N} and \tilde{q} disappear and the three curves coincide. When the curves do not
 482 coincide, mixing is inhomogeneous, and the coincidence of the curves indicates that the mixing
 483 becomes homogeneous. In Fig. 5a and 5b ($Da = 1$ and $Da = 5$, respectively), the curves
 484 coincide at point A corresponding to time $\tilde{t} = T_{mix}$.

485 Figs. 5a,b show that at $Da = 1$ and $Da = 5$, mixing consists of two stages: inhomogeneous
 486 and homogeneous. The time instance $\tilde{t} = T_{mix}$ separates these two stages. In turn, the period of
 487 homogeneous mixing (when evaporation is spatially homogeneous) can be separated into two
 488 sub-periods. During the first sub-period, droplets evaporate only partially and \tilde{q} decreases at
 489 the same droplet concentration. This sub-period is very pronounced at $Da = 1$, when \tilde{q}
 490 decreases from about 0.4 to 0.1 at the unchanged droplet concentration. At the second sub-
 491 period, when $\tilde{q} < 0.1$, droplets evaporate completely, beginning with smaller ones, so both the
 492 droplet concentration and \tilde{q} rapidly drop to zero. At $Da = 5$ (Fig. 5b), at the stage of
 493 homogeneous evaporation (that begins at point “A”) the decrease in \tilde{q} is accompanied by a
 494 decrease in \tilde{N} .

495 At $Da = 50$ (Fig 5c), curves corresponding to different values of \tilde{x} do not coincide, except
 496 at the final point “F”, where $\tilde{N} = 0$ and $\tilde{q} = 0$. This means that horizontal gradients exist during
 497 the entire mixing process and mixing is inhomogeneous till the final equilibrium state is
 498 reached. Droplets penetrating into the initially droplet-free volume begin evaporating, so only a
 499 small fraction of droplets reaches the centre of the droplet-free volume, as seen in Fig. 5c,
 500 $\tilde{x} = 3/4$ (black curve). Accordingly, at $\tilde{x} = 3/4$ the droplet concentrations and \tilde{q} reach their
 501 maxima (of 0.1 and 0.05, respectively) and then decrease to zero. At $Da = 500$ (Fig 5d), all
 502 the droplets evaporate before reaching the centre of the dry volume, indicating an extremely
 503 high spatial inhomogeneity of droplet evaporation. Hence, only two curves for $\tilde{x} = 1/4$ and
 504 $\tilde{x} = 1/2$ are seen in Fig.5d.

505 Fig. 5 also shows that the slopes of the curves describing the $\tilde{N} - \tilde{q}$ relationships are
 506 different at different values of \tilde{x} and change over time. At large Da , the slopes of the curves
 507 describing the dependencies $\tilde{N} - \tilde{q}$ in the initially cloud volume are close to linear. However,
 508 the slope at a high value of \tilde{q} is still flatter than that at a low value of \tilde{q} . This can be attributed
 509 to the fact that when \tilde{q} is large, it decreases faster than the concentration \tilde{N} because some

510 fraction of droplets evaporate only partially. At the end of the mixing when \tilde{q} is small, \tilde{N}
 511 decreases faster than \tilde{q} , because the droplet concentration is determined by the smallest
 512 droplets, while \tilde{q} is determined by larger droplets.

513 As was discussed in Pt. 1, according to the classical concept of extremely inhomogeneous
 514 mixing, the ratio q/N remains constant. For dimensionless \tilde{N} and \tilde{q} , the scattering points
 515 should be aligned along the 1:1 line. Therefore, the closeness of particular cases to the classical
 516 extremely inhomogeneous mixing can be evaluated by the deviation of the $\tilde{N}-\tilde{q}$ curve from
 517 the 1:1 line. One can see that at $Da = 500$ the $\tilde{N}-\tilde{q}$ relationship is closer to linear.

518 Despite the fact that at $R < -1$ all the droplets within the mixing volume evaporate, it is
 519 interesting to follow the DSD evolution during this process. **Figure 6** shows the time evolution
 520 of a normalized DSD at $Da = 1$ and $Da = 50$. One can see a substantial difference in the DSD
 521 evolutions at different Da . At $Da = 1$, different DSDs are formed very rapidly at different
 522 values of \tilde{x} (panel a). The widest DSD occurs at $\tilde{x} = 1$, i.e. at the outer boundary of the initially
 523 droplet-free volume. This is natural, because the supersaturation deficit is the highest at $\tilde{x} = 1$.
 524 At $\tilde{t} > T_{mix} \approx 0.4$, DSD become similar at all values of \tilde{x} (Fig.6b). The DSD width continues to
 525 increase due to partial droplet evaporation. This time period corresponds to the horizontal
 526 segment of the $\tilde{N}-\tilde{q}$ relationship in Fig. 5a. Fig. 6c shows the DSD at the stage when a
 527 decrease in LWC is accompanied by a decrease in number droplet concentration. The
 528 corresponding point in the $\tilde{N}-\tilde{q}$ diagram at this time instance is quite close to the point “F” at
 529 which $\tilde{N} = 0$ and $\tilde{q} = 0$.

530 At $Da = 50$, DSD are different at different \tilde{x} during the entire period of mixing. While
 531 DSD at $\tilde{x} > 0.5$ are wide and droplet evaporation is accompanied by a shift of DSD maximum
 532 to smaller droplet radii (this feature is typically attributed to homogeneous mixing), the DSD
 533 maximum at $\tilde{x} < 0.5$ (the initially cloud volume) shifts toward smaller radii only slightly until
 534 $\tilde{t} = 3.17$ (Fig. 6e). Further droplet evaporation either leads to a complete evaporation (at

535 $\tilde{x} \geq 0.5$) or shifts the DSDs to smaller droplet sizes (panel f). The maximum droplet
 536 concentration takes place at $\tilde{x} = 0$. Fig. 6 shows that DSD shapes evolve substantially over
 537 time, although the final state is characterized by complete droplet evaporation.

538

539 **5.2 Partial evaporation case**

540 **5.2.1 Evolution of the microphysical parameters at different values of Da and R**

541 Here we consider the process of mixing at $R > -1$, i.e. when not all the droplets evaporate
 542 completely. **Figure 7** shows the horizontal profiles of a normalized supersaturation at different
 543 Da and R . One can see that in all cases, the final state occurs when the equilibrium
 544 supersaturation $\tilde{S} = 0$ (RH=100%). However, this final value is reached quite differently
 545 depending on Da . At $Da = 1$, rapid mixing leads to formation of spatially homogeneous
 546 humidity and supersaturation during a time period of a fraction of τ_{pr} . Then, supersaturation
 547 within the mixing volume grows by evaporation of droplets, which are uniformly distributed
 548 over the entire mixing volume. This process of homogeneous mixing was analyzed in detail in
 549 Pt. 2.

550 At $Da = 500$, changes in supersaturation take place largely within the initially droplet-free
 551 volume. RH in the initially cloud volume undergoes only small changes. This process agrees
 552 well with the classical concept of extremely inhomogeneous mixing. However, a strong
 553 gradient of supersaturation remains within the initially drop-free volume for a long time (tens
 554 of τ_{pr}). At $Da = 50$, the situation is intermediate. Mixing is intensive enough to decrease RH
 555 in the initially cloud volume, but spatially uniform RH is established within about $5-10\tau_{pr}$,
 556 increasing with an increase in $|R|$. After this time instance, mixing takes place according to the
 557 homogeneous scenario.

558 **Figure 8** shows the horizontal profiles of normalized LWC at different Da and R . At the
 559 same R , the final equilibrium values of LWC are identical, as follows from Eq. (30); LWC

560 decreases with an increase in $|R|$. At any Da , the decrease in the LWC in the cloud volume is
 561 caused largely by diffusion of droplets from the cloud volume into the initially droplet-free
 562 volume .

563 At $Da = 500$, evaporation in the cloud volume is small because \tilde{S} in these volumes is high
 564 in cloud volumes during mixing (Fig. 7). At $Da = 1$, the process of spatial homogenization
 565 takes place during fractions of τ_{pr} , i.e. $T_{mix} < 1$. Then, during a relatively lengthy period of
 566 $10\tau_{pr}$, evaporation decreases LWC over the entire mixing volume, which is characteristic of
 567 homogeneous mixing. At $Da = 50$, spatial homogenization takes place during about $T_{mix} \approx 15$.
 568 This is a slightly shorter time than it takes to establish the final equilibrium stage T_{tot} . Different
 569 Da 's cases reach equilibrium at different times. The process of reaching a final uniform LWC
 570 lasts for $100\tau_{pr}$ at $Da = 500$ and for about τ_{pr} at $Da = 1$.

571 **Figure 9** shows the profiles of the normalized droplet concentrations at different Da and
 572 R . In contrast to LWC, the final concentration depends both on Da and R . Hence, profiles at
 573 different Da can have different shapes at the same value of R . At $R = -0.1$ (which corresponds
 574 to high RH in the initially dry volume) none of the droplets evaporate, so the final normalized
 575 droplet concentration is equal to $\tilde{N} = 1/2$. This means that all the droplets in the initially cloud
 576 volume are now uniformly distributed between both mixing volumes. At larger $|R|$, i.e., at
 577 lower RH in an initially droplet-free volume, some droplets evaporate completely. The final
 578 concentration decreases with an increase in Da .

579 The physical interpretation of this dependence is clear. At low Da , fast mixing leads to
 580 formation of a uniform RH throughout the entire mixing volume, and this affects all the
 581 droplets. At high Da , RH in the initially droplet-free volume remains low for a long time,
 582 and droplets that penetrate can evaporate. Therefore, the fraction of completely evaporated
 583 droplets increases with Da : at $R = -0.1$ there are no completely evaporated droplets at any Da .

584 At $R = -0.3$ a decrease in the droplet concentration takes place only at $Da = 500$, and at
 585 $R = -0.5$ the droplet concentration decreases already at $Da \geq 50$.

586 The comparative contributions of different factors in establishing the final states of mixing
 587 are well seen in **Figure 10** presenting the relationships between normalized concentration and
 588 normalized LWC at three values of \tilde{x} : $1/4$ (centre of the cloudy volume), $1/2$ and $3/4$ (centre of
 589 the initially dry volume) at $R = -0.5$ and different values of Da . Fig. 10 is analogous to Fig. 5,
 590 but plotted for $R > -1$.

591 At $Da = 1$ the mixing is very fast, which leads to a rapid decrease in LWC and in the
 592 droplet concentration in the initially cloud volume and to an increase of these quantities in the
 593 initially droplet-free volume. As a result of the rapid mixing and homogenization, all the curves
 594 coincide at point “A” (left panel). After this time instance, spatial homogeneous evaporation
 595 takes place. Since at $Da = 1$ only partial, but not total, droplet evaporation occurs, the droplet
 596 concentration remains unchanged even while LWC decreases. At $Da = 50$ and $Da = 500$, the
 597 three curves coincide at the final point “F” only. At $Da = 500$, the relationship between the
 598 droplet concentration and the mass becomes more linear (blue curve). The linear dependence is
 599 consistent with the concept of extremely inhomogeneous mixing (see Pt1). Considerations
 600 regarding the closeness of the $\tilde{N} - \tilde{q}$ relationship to the line 1:1 as a measure of
 601 inhomogeneity of mixing made at $R < -1$ are also valid for $R > -1$.

602

603 **5.2.2 Evolution of DSDs and the DSD parameters**

604 **Figure 11** presents examples of the DSD evolution at the center of the initially cloud
 605 volume ($\tilde{x} = 1/4$) (upper row) and of the initially droplet-free volume ($\tilde{x} = 3/4$) at $R = -0.5$
 606 and different values of Da . Several specific features of the DSD are notable. As a result of the
 607 rapid mixing at $Da = 1$ (left column), DSD become similar in both volumes already at
 608 $t = 0.317\tau_{pr}$ (black lines). Further evolution is similar in both volumes and is characterized by
 609 broadening of the DSD and its shifting and of the DSD toward smaller droplet sizes. This shift

610 means a decrease in the mass at constant droplet concentration, which is typical of
 611 homogeneous mixing.

612 The initially monodisperse DSDs become polydisperse. The mechanism of the DSD
 613 broadening at $Da=1$ is illustrated in **Figure 12**, showing the DSD at the earlier,
 614 inhomogeneous stage at different \tilde{x} . One can see that within very short periods when the
 615 spatial gradient of saturation deficit exists, droplets entering the initially droplet-free volume
 616 partially evaporate, reaching their minimal size at $\tilde{x}=1$. In this way, a polydisperse DSD
 617 forms. As the mixing proceeds, DSD become spatially homogenized, as seen in the right panel
 618 of Fig. 12.

619 At $Da=50$ and $Da=500$, the DSD shapes substantially differ from those at $Da=1$.
 620 There are two main differences: the peak of the distribution shifts only slightly (at $Da=50$) or
 621 does not shift at all (at $Da=500$). At the same time, the DSD develops a long tail of small
 622 droplets. Since the mixing rate at these values of Da is slow, droplets penetrating deeper into
 623 the initially dry volume remain there for long time and get smaller. As a result, at moderate
 624 and large Da , a polydisperse DSDs form with droplet sizes ranging from zero to 1. Formation
 625 of a long tail of small droplets in case of inhomogeneous mixing was simulated in direct
 626 numerical simulation (DNS) by Kumar et al. (2012), as well as by means of “the explicit-
 627 mixing parcel model” (EMPM) (Krueger et al., 1997; Su et al., 1998; Schlüter, 2006).

628 **Figure 13** shows the spatial dependencies of the DSD dispersion (ratio of DSD r.m.s. width
 629 and the mean radius) at different time instances and different values of Da and R . One can see
 630 that the dispersion increases with an increase in Da and in $|R|$. This behavior can be accounted
 631 for by the fact that the DSD broadening toward smallest droplet size increases with the increase
 632 in Da and in $|R|$. The DSD dispersion increases with time and with an increase in \tilde{x} , i.e.
 633 further into the initially droplet free volume. At the same time, spatial homogenization takes
 634 place, so at the final state at $R=-0.5$ the DSD dispersion reaches 0.11 at $Da=1$ and about 0.2
 635 at $Da=50$ and $Da=500$.

636 Observed DSD dispersion in different clouds typically ranges from 0.1 to 0.4 (Khain et al.,
 637 2000; Martin et al., 2004; Prabha et al., 2012) and can be caused the following factors: in-
 638 cloud nucleation (e.g. Khain et al., 2000; Pinsky and Khain, 2002), spatial averaging along
 639 aircraft traverses (Korolev, 1995) and non-symmetry in droplet nucleation/denucleation
 640 (Korolev, 1995). As seen in Fig. 13, this dispersion may be also caused by mixing at cloud
 641 edges at moderate and large Da . Hence, inhomogeneous mixing leads to DSD broadening.

642 The effective radius, r_{eff} , is an important DSD characteristic. According to the classical
 643 concept, r_{eff} remains unchanged during extremely inhomogeneous mixing, whereas decreases
 644 during homogeneous mixing. **Figure 14** shows spatial dependencies of r_{eff} at different time
 645 instances and different values of Da and R . At $R = -0.1$ (high RH in the surrounding volume)
 646 r_{eff} is similar for all values of Da . So, at high R (i.e., close to zero), the behaviour of r_{eff} does
 647 not allow to distinguish between mixing types.

648 At a given R , the final r_{eff} increases with increasing Da . For instance, at $R = -0.5$, r_{eff} at
 649 the final state differs from the initial r_{eff} value by less than 6% at $Da = 500$, while at $Da = 1$
 650 r_{eff} decreases by 20%. At moderate and high Da , large gradients of r_{eff} exist during the
 651 mixing process. However, the gradient is high only in the initially droplet-free volume where
 652 r_{eff} decreases significantly due to the intense evaporation of droplets. Besides, r_{eff} growth very
 653 rapidly in the initially droplet free volume, so at high Da during most of the mixing time r_{eff}
 654 within the mixing volume becomes close to the initial r_{eff} value in the cloudy volume.

655

656 **5.3 Delimitation between mixing types**

657 Typically, the Da value is used as a criterion for delimitation between mixing types.
 658 $Da = 1$ is usually used as a boundary value separating homogeneous and inhomogeneous
 659 mixing. As shown in Section 4, mixing always starts as inhomogeneous. In the course of

660 mixing, the initial spatial gradients decrease and the air volumes either become identical or
 661 remain different. In the former case, the second mixing stage is homogeneous. If
 662 inhomogeneity persists until the equilibrium state is established, mixing remains
 663 inhomogeneous during the entire period. Both mixing stages can be characterized by duration,
 664 change in the droplet concentrations or LWCs, and other quantitative characteristics. These
 665 characteristics are functions of two non-dimensional parameters R and Da , which can be
 666 calculated and used for delimitation between mixing types. Since mixing between volumes
 667 may turn from inhomogeneous into homogeneous before reaching the equilibrium state, it is
 668 necessary to use some quantitative criteria to delimit mixing types. Below, delimitation is
 669 performed for $R > -1$ which corresponds to partial evaporation of droplets by the end of
 670 mixing.

671

672 **5.3.1. Characteristic time periods of mixing**

673 Three characteristic time periods of mixing are distinguished: a) mixing period T_{mix} , during
 674 which spatial gradients are smoothening (may be also called the homogenization period) ; b)
 675 period T_{ev} during which $S < 0$ and droplets evaporate until saturation is reached and c) the total
 676 mixing period T_{tot} that lasts until the final equilibrium stage is reached. In our analysis, all the
 677 three periods are assumed dimensionless quantities.

678 We use solution (28) for conservative function $\tilde{\Gamma}(\tilde{x}, \tilde{t})$ to define quantitatively time period
 679 T_{mix} . The deviation of the solution from its final value $\Delta\tilde{\Gamma} = \tilde{\Gamma}(\tilde{x}, \tilde{t}) - \tilde{\Gamma}(\tilde{x}, \infty)$ at $\tilde{t} \rightarrow \infty$ can be
 680 approximately estimated using the first term of the series expansion as

$$681 \quad \left| \Delta\tilde{\Gamma} \right|_{\max} \approx \left| (1-R) \frac{\sin(\pi/2)}{\pi/2} \exp\left(-\frac{\pi^2 \tilde{t}}{Da}\right) \cos(\pi \tilde{x}) \right|_{\max} = \quad (37)$$

$$(1-R) \frac{2}{\pi} \exp\left(-\frac{\pi^2 \tilde{t}}{Da}\right)$$

682 From Eq. (37) the estimation of T_{mix} can be written as

683

$$684 \quad T_{mix} = -\frac{Da}{\pi^2} \ln \left[\frac{\pi}{2(1-R)} \left| \Delta \tilde{\Gamma} \right|_{\max} \right] \quad (38a)$$

685 Suppose the value of the maximum deviation is $\left| \Delta \tilde{\Gamma} \right|_{\max} = 0.02$. This is a small value
 686 compared to the initial leap of function $\tilde{\Gamma}$, which is equal to $1-R$. At $\left| \Delta \tilde{\Gamma} \right|_{\max} = 0.02$ the
 687 duration of the non-homogeneous stage is evaluated as

$$688 \quad T_{mix} = -\frac{Da}{\pi^2} \ln \left[\frac{0.01\pi}{1-R} \right] \quad (38b)$$

689

690 Several studies evaluate the evaporation time for droplets of a particular size using the
 691 equation for diffusion growth (e.g. Lehmann et al., 2009). In our study, the evaporation time
 692 duration T_{ev} is defined as the period during which the maximum deviation of supersaturation
 693 from zero exceeds the small value chosen as $\left| \Delta \tilde{S} \right|_{\max} = 0.02$:

$$694 \quad \left| \tilde{S}(\tilde{x}, T_{ev}) \right| \leq \left| \Delta \tilde{S} \right|_{\max} = 0.02 \quad (39)$$

695

696 Although criterion (39) is rather subjective, it has an advantage over the criterion used by
 697 Lehmann et al. (2009), as Eq. (32) characterizes evaporation of the droplet population taking
 698 into account the simultaneous increase in supersaturation, but not of individual droplets of
 699 particular size at constant S as in Lehmann et al. (2009).

700

701 At the end of the mixing, both the thermodynamic equilibrium and the diffusion
 702 equilibrium are reached. Accordingly, the total time of mixing T_{tot} is evaluated as the
 703 maximum of the two time periods needed to achieve equilibrium $T_{tot} = \max \{ T_{mix}, T_{ev} \}$. All the
 704 three characteristic time periods are normalized on the phase relaxation time, and, therefore,
 705 depend on the two non-dimensional parameters R and Da . The contours of the characteristic
 time durations T_{mix} , T_{ev} and T_{tot} in the $Da-R$ diagrams are shown in **Figure 15**.

706 As follows from Eq. (38b), T_{mix} is proportional to Da . The dependence of T_{mix} on R is not
 707 very strong, so T_{mix} slightly decreases with increasing R . This can be attributed to the fact that
 708 the lower R , the smaller the initial inhomogeneity of function $\tilde{\Gamma}$ and the shorter the time to
 709 align this inhomogeneity is. At small Da (high rate of homogenization of the volume), T_{ev}
 710 depends largely on R . At large Da , T_{ev} depends substantially on Da , since the evaporation
 711 rate depends on the number of droplets that diffuse to drier parts of the mixing volume. A
 712 comparison of Fig. 15c with Figs. 15a and 15b shows that at small Da , time T_{tot} is determined
 713 by T_{ev} , while at large Da , T_{tot} is determined by T_{mix} .

714

715 **5.3.2. Determination of boundaries between the mixing types on the $R-Da$ plane**

716 Several criteria can be proposed for delimitation between mixing types. We consider these
 717 criteria for $R > -1$. As discussed above, mixing always starts as inhomogeneous and late either
 718 become homogeneous or remains inhomogeneous till the final equilibrium state is established.
 719 At small Da , the homogenization takes place during $T_{mix} < T_{tot}$. The value of time fraction λ_1 of
 720 the inhomogeneous stage can serve as a criterion for definition of homogeneous mixing. This
 721 formula for the fraction can be written as

$$722 \lambda_1 = \frac{T_{mix}}{T_{tot}} \quad (40)$$

723 The case $\lambda_1 \leq 0.5$, most time the mixing takes place according the homogeneous scenario and
 724 such regime is reasonable to regard as homogeneous mixing. If $\lambda_1(R, Da)$ changes within the
 725 range of $0.5 < \lambda_1 \leq 1$, mixing appears to be intermediate. The criterion (40) depends on the non-
 726 dimensional parameters R and Da . **Figure 16a** shows the boundaries separating mixing types
 727 on the $Da-R$ plane. These boundaries separate all plane into several zones. At very small R ,
 728 the duration of the phase transition is negligibly small. According to criterion (40), in this case
 729 mixing should be considered inhomogeneous, irrespective of the Da value.

730 Another criterion of delimitation between mixing types can be determined from a
 731 comparison of LWC variation rates due to different mechanisms. The mean normalized LWC
 732 (which is equal to the mean normalized liquid water mixing ratio) can be written as integral

733 $\langle \tilde{q}(\tilde{t}) \rangle = \int_0^1 \tilde{q}(\tilde{x}, \tilde{t}) d\tilde{x}$. The initial mean LWC is equal to $\langle \tilde{q}(t=0) \rangle = \frac{1}{2}$. The final equilibrium

734 LWC is equal to $\langle \tilde{q}(t=\infty) \rangle = \frac{1}{2}(1+R)$ (Eq. (30)). The total amount of liquid water that

735 evaporates in the course of mixing can be quantified by the difference between these two

736 values $\langle \tilde{q}(t=0) \rangle - \langle \tilde{q}(t=\infty) \rangle = -\frac{1}{2}R$. The amount of liquid water evaporated in the course of the

737 first inhomogeneous mixing stage is calculated by the equation

738 $\langle \tilde{q}(t=0) \rangle - \langle \tilde{q}(T_{mix}) \rangle = \frac{1}{2} - \langle \tilde{q}(T_{mix}) \rangle$. Hence, parameter λ_2 which is a ratio of

739

$$740 \lambda_2 = \frac{\langle \tilde{q}(t=0) \rangle - \langle \tilde{q}(T_{mix}) \rangle}{\langle \tilde{q}(t=0) \rangle - \langle \tilde{q}(t=\infty) \rangle} = \frac{2\langle \tilde{q}(T_{mix}) \rangle - 1}{R} \quad (41)$$

741 can serve as another possible criterion for delimitation between mixing types. This ratio

742 characterizes the fraction of liquid water that evaporates at the initial inhomogeneous stage.

743 Condition $\lambda_2 < 0.5$ in this case corresponds to homogeneous mixing, while condition

744 $0.5 \leq \lambda_2 < 1$ corresponds to intermediate mixing. We regard the case $\lambda_2 = 1$ as inhomogeneous

745 mixing. Certainly, criterion λ_2 depends on the non-dimensional parameters R and Da . Fig.

746 16b illustrates delimitation between mixing types on the $Da-R$ plane according to criterion

747 λ_2 .

748 Comparison of Figs. 16a and 16b shows that both criteria lead to nearly similar separation

749 of the $Da-R$ plane into three zones corresponding to homogeneous, intermediate and

750 inhomogeneous mixing. At the same time, the boundaries separating these zones are different

751 depending on the delimitation criterion used. Nevertheless, it can be concluded that mixing can

752 be considered homogeneous at Da below 4-10 and $R < -0.1$ and inhomogeneous at Da
 753 exceeding several tens.

754 Terms "inhomogeneous mixing" (Burner and Brenguier, 2007) and "extremely
 755 inhomogeneous mixing" (Lehmann et al., 2009; Gerber et al., 2008; Pt1) are used to denote the
 756 mixing regime when the relationship between the normalized values \tilde{N} and \tilde{q} is represented
 757 by a straight 1:1 line, which is equivalent to the constant mean volume radius (in some studies,
 758 the effective radius is used instead of the mean volume radius. According to the definition used
 759 in the present study, extremely inhomogeneous mixing is the limiting case of inhomogeneous
 760 mixing when $Da \rightarrow \infty$. Despite the fact that the extremely inhomogeneous mixing is only an
 761 idealization our approach allows to determine to what extent mixing can be considered to be
 762 close to this limiting case. The measure of inhomogeneity of mixing is the closeness of the
 763 $\tilde{N} - \tilde{q}$ relationship to the 1:1 straight line (see discussion above related to Figs. 5 and 10).

764 **Figure 17a** shows r.m.s. distance between the $\tilde{N} - \tilde{q}$ relationship and the 1:1 straight line,
 765 depending on Da and R . These dependences were calculated using the set of points \tilde{N}_i, \tilde{q}_i
 766 uniformly distributed over spatial interval $[0, 1]$ and time interval $[0, T_{tot}]$. The equation for

767 estimation is $\delta = \sqrt{\frac{1}{2M} \sum_{i=1}^M (\tilde{N}_i - \tilde{q}_i)^2}$, where M is the total number of points. This distance

768 corresponds to r.m.s. deviation of the normalized mean volume radius from 1. The dependences
 769 of the last deviation on Da and R and estimated as $\delta/3$ are shown in Fig. 17b. This estimation
 770 is based on the fact that the total mass of droplets is proportional to the cube of the mean
 771 volume radius. As expected, the distance decreases with increasing in Da . At large R , all the
 772 curves coincide indicating a degenerative case when type of mixing becomes indistinguishable.

773 We choose the value $\delta/3$ equal to 0.02 to determine the boundary of the extremely
 774 inhomogeneous mixing zone. The value of 0.02 corresponds to droplet radii deviation of a few
 775 tenths of a micron, which is so low that in in-situ measurements this case would always be
 776 attributed to extremely inhomogeneous mixing. In Fig.16 this boundary is marked by broken

777 line. The boundary shows that the mixing at Da exceeding several hundred can be attributed
778 to the extremely inhomogeneous. Between the boundary separating inhomogeneous mixing
779 from the intermediate one and the boundary separated inhomogeneous mixing from extremely
780 inhomogeneous there exists a wide zone of inhomogeneous mixing where the mean volume (or
781 the effective) radius may drop by 10% and more (Fig. 14), and where the DSD dispersion is
782 substantial and the tail of small droplets is long enough (Fig. 11). Mixing diagrams currently
783 used for analysis of observed data ($N-q$ dependences in the final equilibrium state of mixing)
784 do not contain this zone which, therefore, has remained unrecognized and uninvestigated.

785

786 **6. Summary and conclusions**

787 In this study, inhomogeneous turbulent mixing is investigated using a simple a 1D model of
788 mixing between a saturated cloud volume and an undersaturated droplet-free volume. The
789 mixing is simulated by solving a diffusion-evaporation equation written in the non-dimensional
790 form. For simplicity, the initial volumes of cloudy and droplet-free air were assumed to be
791 equal, and the initial DSD in the cloudy volume was assumed monodisperse.

792 Analysis of the diffusion-evaporation equation shows that the time-dependent process of
793 mixing and the final equilibrium state depend on two non-dimensional parameters. The first
794 parameter R , referred in this paper as potential evaporation parameter (PEP) is proportional to
795 the ratio between the saturation deficit in the initially droplet-free volume and the initial liquid
796 water content in the cloudy volume. At $R < -1$, the final state is characterized by complete
797 droplet evaporation and a spatially homogeneous saturation deficit, which indicates dissipation
798 of the cloudy volume. At $R > -1$, the final state is characterized by existence of droplets and
799 zero saturation deficit (RH=100%). In this case, the cloud volume expands after mixing with the
800 entrained air. At small values of $|R|$ (e.g., when RH in the entrained volume is close to 100%),
801 the effect of droplet evaporation on microphysics is small, and, formally, this kind of mixing
802 should be regarded as extremely inhomogeneous. Strictly speaking, this is a degenerate case,

803 when homogeneous and inhomogeneous mixing cannot be distinguished (see also Pt. 1). At
 804 $R = 0$, the droplet population turns into a passive admixture and its turbulent diffusion will be
 805 the same as different thermodynamic parameters.

806 The second parameter is the *Damköhler* number (Da) which is the ratio between the
 807 characteristic mixing time and the phase relaxation time. This parameter compares the rates of
 808 spatial diffusion and evaporation. Parameter Da (Eq. (23)) is logically appears in the non-
 809 dimensional form of the diffusion-evaporation equation showing that Da is the ratio of the
 810 mixing time defined as $\tau_{mix} = \frac{L^2}{K}$, to the initial drop relaxation time. The expression for this non-
 811 dimensional parameter clearly shows that since we consider an ensemble of evaporating droplets,
 812 the drop relaxation time evaluated just before the mixing is the characteristic time scale of
 813 inhomogeneous mixing process. In several studies (e.g., Baker and Latham, 1979; Burnet and
 814 Brenguier, 2007; Andejchuk et al., 2009) a question was raised as to which time scale should be
 815 used in formulation of the *Damköhler* number: the time of an individual droplet evaporation at
 816 constant saturation deficit, or the phase relaxation time. This study, as well Pt. 2 show that the
 817 phase relaxation time is the answer. The mixing time is introduced via the turbulent diffusion
 818 coefficient which is a natural measure characterizing the diffusion rate and, in particular,
 819 determines the propagation rate of the fronts in the fields of droplet concentration and other
 820 microphysical parameters. The turbulent diffusion coefficient is widely used to describe mixing
 821 in cloud models at resolved scales.

822 The analysis was performed within a wide range of Da (from 1 to 500) and of R (from -
 823 1.5 to -0.1). The final LWC and the humidity in the mixing volume are determined by the mass
 824 conservation and do not depend on Da (see also Pt. 1 and Pt. 2). At the same time, the droplet
 825 concentration, as well as the shape of DSD and their parameters strongly depend on Da .

826 It is shown that the mixing of air volumes with initially different thermodynamical and
 827 microphysical parameters consists of two stages characterized by two time periods: the time

828 during which microphysical characteristics become uniform over the total mixing volume T_{mix} ,
 829 and the time during which zero saturation deficit is reached (at $R > -1$), T_{ev} . At $\tilde{t} < T_{mix}$, the
 830 spatial gradients of the microphysical values remain and the mixing regime can be regarded as
 831 inhomogeneous. At $\tilde{t} > T_{mix}$, droplet evaporation, if it occurs at all, takes place within a
 832 spatially homogeneous medium, so all the droplets in the mixing volume experience equal
 833 saturation deficit. This regime can be regarded as homogeneous. It is shown, therefore, that at
 834 small Da mixing between two volumes that starts as inhomogeneous can become
 835 homogeneous towards the end of mixing.

836 This finding allows to delimit between mixing types. We presented two quantitative criteria
 837 on the $Da-R$ plane that allow to delimit three mixing regimes: homogeneous, intermediate
 838 and inhomogeneous. These criteria are based on comparison of the characteristic duration
 839 mixing and the evaporation rates. According to the criteria, at Da below about 5, mixing can
 840 be regarded as homogeneous, i.e. the main microphysical changes take place during the
 841 homogeneous stage. At $5 < Da < 50$, the changes in the microphysical parameters are more
 842 significant at the inhomogeneous stage than at the homogeneous stage. In this case, the mixing
 843 can be regarded as intermediate. Finally, at Da exceeding several tens, the spatial
 844 microphysical gradients remain until the final equilibrium stage is reached. In this case, the
 845 mixing can be regarded as inhomogeneous. At Da exceeding a few hundred the deviations
 846 from predictions based of the classical concept of extremely inhomogeneous become relatively
 847 small, which justifies attribute regarding this mixing as extremely inhomogeneous.

848 On the whole, the results of the present study are in line with the classic concepts defining
 849 homogeneous and inhomogeneous mixing types. However, several important points emerge
 850 from our work show serious limitations of classical concepts. A comparison of the classical
 851 concepts and the present study is presented in **Table 2**. Analysis of Tab. 2 shows the following.

852 a) In contrast to many studies that analyze only the hypothetical final (equilibrium) state of
 853 mixing (Barnet and Brenguier, 2007; Gerber et al., 2008; Morrison and Grabowski, 2008; Hill

854 et al., 2009), we consider the entire time-dependent processes of mixing and evaporation. At
 855 moderate and high Da , the mixing can last several minutes. In in-situ observations, we see
 856 mostly non-equilibrium stages which may account for a rather wide scattering of mixing
 857 diagrams even at the same values of Da (e.g., Lehmann et al., 2009).

858 Note that time dependent mixing was also considered in several studies (e.g. Baker et al.,
 859 1980; Baker and Latham, 1982; Jeffery and Reisner, 2006; Krueger et al., 1997; Kumar et al.,
 860 2012) using different approaches and numerical models. These studies, however, do not contain
 861 analysis on non-dimensional diffusion-evaporation equation.

862 b) It is also shown in the study that the slopes of the $\tilde{N} - \tilde{q}$ relationship (between the
 863 normalized droplet concentration and LWC) tends to the 1:1 line with increasing Da . The
 864 closeness can be considered as a measure of extremely inhomogeneous mixing in terms of the
 865 classical concept (see Pt. 1). It has been found that the slope of the $\tilde{N} - \tilde{q}$ relationship depends
 866 on the LWC and, accordingly, on time. At large LWC, \tilde{q} changes with time faster than \tilde{N} ,
 867 while at low LWC the concentration changes faster. Although mixing types are usually
 868 separated into homogeneous and extremely inhomogeneous, we have shown that there are wide
 869 ranges of Da and R at which mixing should be considered intermediate or inhomogeneous,
 870 but not extremely inhomogeneous. Within these ranges the effective radius can change by more
 871 than 10-15%. Standard mixing diagrams do not include this range that, to our knowledge, has
 872 never been investigated despite the fact that multiple in-situ measurements indicate its
 873 existence (e.g. Lu et al. 2014)

874 c) Many studies assume the existence of pure homogeneous mixing during which the
 875 initially monodisperse DSD remains monodisperse. Our study shows that at the very beginning,
 876 mixing is always inhomogeneous. This inhomogeneous stage leads to formation of a
 877 polydisperse DSD that broadens in the course of droplet evaporation. Hence, even at $Da = 1$
 878 the initially monodisperse spectrum becomes polydisperse.

879 d) It is shown that at small Da , mixing includes both inhomogeneous and homogeneous
880 stages, which means that type of mixing can change during the mixing process.

881 e) The classical concept assumes that the effective radius always decreases during
882 homogeneous mixing. Assuming an initially monodisperse DSD, we have found this
883 conclusion largely valid, with the exception small R . At the same time, it was shown in Pt. 2
884 that during homogeneous mixing, the effective radius can decrease, remain constant or increase
885 depending of the initial DSD shape. Thus, a decrease in the effective radius during mixing
886 cannot always be considered an indication of homogeneous mixing. Similarly, the invariability
887 the effective radius during mixing in the process cannot always be considered an indication of
888 extremely inhomogeneous mixing.

889 f) It is generally assumed that during homogeneous mixing droplet concentration remains
890 unchanged. In the present study, as well as in Pt. 2, it is shown that since mixing leads to a
891 polydisperse DSD, the smallest droplets may completely evaporate. At $R < -1$, the DSD
892 becomes very wide and all the droplets, the smallest ones first, evaporate.

893 g) It is generally assumed that inhomogeneous mixing does not alter DSD shape, but only
894 decreases droplet concentration. The present study showed that inhomogeneous mixing
895 significantly changes the DSD shape. DSD were found to be quite different in different regions
896 of mixing volumes. The main feature is the DSD broadening toward small droplet size, so the
897 relative dispersion grows up to 0.2-0.3. These values are quite close to those observed in
898 atmospheric clouds (Khain et al., 2000). Elongated tails of small droplets during mixing were
899 simulated by Schlüter (2006) who described turbulent diffusion following to Kruger et al.,
900 (1997) and Su et al., (1998) as well as by Kumar et al. (2012) using DNS. We see that
901 formation of a polydisperse DSD is a natural result of inhomogeneous mixing and, therefore,
902 inhomogeneous mixing is an important mechanism of DSD broadening. A significant impact
903 of mixing on DSD shape was found identified in multiple studies, beginning with Warner
904 (1973).

905 h) The effective radius has been assumed to remain constant during extremely
906 inhomogeneous mixing. Our results indicate that, indeed, at the final equilibrium stage at
907 comparatively high RH the effective radius is close to that in the initially cloudy volume
908 (especially at high Da). At the same time, we found that the effective radius varies in size and
909 is smaller in the initially droplet-free volumes.

910 The results obtained in parts Pt1 and Pt 2, and especially in the current study (Pt 3)
911 dedicated to analysis of turbulent mixing mechanisms in clouds determine the directions for
912 future work. Since the widely used mixing diagrams show only a hypothetical equilibrium
913 state, but not the instantaneous state of mixing that likely correspond to transition periods, the
914 efficiency of the standard mixing diagrams is questionable. Moreover, the standard diagrams
915 miss a very important mixing regime, namely, inhomogeneous mixing that occurs between two
916 limiting cases of homogeneous and extremely inhomogeneous mixing (Fig. 16).

917 We believe that the results obtained will help to improve understanding and interpretation
918 of mixing process both in in-situ measurements and modeling. The approach allows to
919 investigate the relationship between the main microphysical parameters typical of
920 inhomogeneous mixing, that differ from those in the limiting cases of extremely
921 inhomogeneous mixing. In addition, utilization of polydisperse DSD when solving diffusion-
922 evaporation equation allows to investigate the role of the initial DSD shape in mixing. In-situ
923 measurements (e.g., Burnet and Brenguier, 2007; Gerber et al., 2008; Lehmann et al., 2009)
924 and numerical models (Magaritz-Ronen et al., 2016) show a wide scattering of data on the
925 scattering diagrams. We expect location of various points on the diagrams (e.g. r_v^3 vs. dilution
926 rates) depends on the shape of the initial DSDs and characterizes the stage of mixing. The
927 method applied in the study allows investigation of evolution of DSD moments over space and
928 time .

929 Recently, there has been vigorous discussions concerning the possible existence of high
930 humidity layer near cloud edges that might affect mixing of cloud with its surrounding (Gerber

931 et al., 2008; Lehmann et al., 2009). In our opinion, this layer does exist and forms as a result of
932 turbulent mixing of cloud with surrounding dry air, accompanied by complete droplet
933 evaporation. The approach developed in the present paper allows to analyze formation of such
934 humid layers.

935 We believe that the results obtained in this study will foster the development of physically
936 grounded parameterization of mixing in cloud models.

937

938 *Acknowledgements*

939 This research was supported by the Israel Science Foundation (grant 1393/14), the Office of
940 Science (BER), the US Department of Energy Award DE-SC0006788 and the Binational US-
941 Israel Science Foundation (grant 2010446). Dr. Korolev's participation was supported by
942 Environment Canada.

943

944

945 **Appendix. List of symbols**

946

947 **Table A here**

948

949

950

951

952

953

954

955

956

957 **References**

958 Andrejczuk M., W. Grabowski, S. P. Malinowski, P. K. Smolarkiewicz, 2009: Numerical
 959 Simulation of Cloud–Clear Air Interfacial Mixing: Homogeneous versus Inhomogeneous
 960 Mixing. *J. Atmos. Sci.*, **66**, 2993-2500.

961 Baker, M., and J. Latham: The evolution of droplet spectra and the rate of production of
 962 embryonic raindrops in small cumulus clouds. *J. Atmos. Sci.*, **36**, 1612–1615, 1979.

963 Baker, M., R. G. Corbin, and J. Latham: The influence of entrainment on the evolution of
 964 cloud drop spectra: I. A model of inhomogeneous mixing. *Quart. J. Roy. Meteor. Soc.*, **106**, 581–
 965 598, 1980.

966 Baker M. B. and J. Latham: A diffusive model of the turbulent mixing of dry and cloudy
 967 air *Quart. J. R. Met. Soc.*, **108**, 871-898, 1982

968 Burnet, F., and J.-L. Brenguier, Observational study of the entrainment-mixing process in
 969 warm convective cloud, *J. Atmos. Sci.*, 64, 1995–2011, 2007.

970 Blyth, A. M., Choularton, T. W., Fullarton, G., Latham, J., Mill, C. S., Smith, M. H., and
 971 Stromberg, I. M.: The Influence of entrainment on the evolution of cloud droplet spectra. 2.
 972 Field experiments 5 at Great Dun Fell, *Q. J. Roy. Meteor. Soc.*, **106**, 821–840, 1980.

973 Boffetta G. and I. M. Sokolov: relative dispersion in fully developed turbulence: The
 974 Richardson’s law and intermittency correction. *Phys. Rev. Let.*, **88**, 094501, 2002.

975 Denvich B. J., P. Bartello, J.-L. Brenguier, L.R. Collins, W.W. Grabowski, R.H.A.
 976 Ijzermans, S.P. Malinowski, M.W. Reeks, J.C. Vassilicos, L-P. Wang, and Z. Warhaft: Droplet
 977 growth in warm turbulent clouds. *Q. J. Roy. Meteorol. Soc.*, **138**, 1401-1429, 2012

978 Gerber H, Frick G, Jensen J.B, and Hudson J.G.: Entrainment, mixing, and microphysics in
 979 trade-wind cumulus. *J. Meteorol. Soc. Jpn.*, **86A**. 87-106, 2008.

- 980 Hill, A. A., G. Feingold, and H. Jiang: The Influence of Entrainment and Mixing
 981 Assumption on Aerosol–Cloud Interactions in Marine Stratocumulus. *J. Atmos. Sci.*, **66**, 1450–
 982 1464, 2009.
- 983 Jeffery, C.A., and J.M. Reisner: A study of cloud mixing and evolution using PDF methods.
 984 Part I: Cloud front propagation and evaporation. *J. Atmos. Sci.*, **63**, 2848-2864, 2006.
- 985 Khain, A. P., M. Ovchinnikov, M. Pinsky, A. Pokrovsky, and H. Krugliak: Notes on the
 986 state-of-the-art numerical modeling of cloud microphysics. *Atmos. Res.* **55**, 159-224, 2000.
- 987 Korolev, A.V.: The influence of supersaturation fluctuations on droplet size spectra
 988 formation. *J. Atmos. Sci.*, **52**, 3620-3634, 1995.
- 989 Korolev A., and I. Mazin: Supersaturation of water vapor in clouds, *J. Atmos. Sci.*, **60**,
 990 2957-2974, 2003.
- 991 Korolev A., A. Khain, M. Pinsky, and J. French: Theoretical study of mixing in liquid
 992 clouds. Part 1: classical concept. *Atmos. Chem. Phys.* , 2015 (submitted)
- 993 Kovetz, A., and B. Olund: The effect of coalescence and condensation on rain formation in
 994 a cloud of finite vertical extent. *J. Atmos. Sci.*, **26**, 1060–1065, 1969.
- 995 Krueger S., C.-W. Su and P. McMurry: Modeling entrainment and finescale mixing in
 996 cumulus clouds. *J. Atmos. Sci.*, **54**, 2697-2712, 1997
- 997 Kumar B., F. Janetzko, J. Schumacher, and R. A. Shaw: Extremely responses of a coupled
 998 scalar-particle system during turbulent mixing. *New J. of Phys.* **14**, 115020 , 2012
- 999 Latham, J. and Reed, R. L.: Laboratory studies of effects of mixing on evolution of cloud
 1000 droplet spectra, *Q. J. Roy. Meteor. Soc.*, **103**, 297–306, 1977.
- 1001 Lehmann, K., H. Siebert, and R. A. Shaw: Homogeneous and inhomogeneous mixing in
 1002 cumulus clouds: Dependence on local turbulence structure. *J. Atmos. Sci.*, **66**, 3641-3659, 2009.
- 1003 Lu, C., Y. Liu, S. Niu, and S. Endo (2014), Scale dependence of entrainment-mixing
 1004 mechanisms in cumulus clouds, *J. Geophys. Res. Atmos.*, 119, 13,877–13,890, doi:10.1002/
 1005 2014JD022265.

- 1006 Magaritz-Ronen L., A. Khain and M. Pinsky, 2016: About the Horizontal Variability of
1007 Effective Radius in Stratocumulus Clouds. *J. Geophys. Res.* (in revision)
- 1008 Martin G.M., D. W. Johnson and A. Spice: The measurements and parameterization of
1009 effective radius of droplets in warm stratocumulus clouds. *J. Atmos. Sci.*, **51**, 1823-1842, 1994.
- 1010 Monin, A.S. and Yaglom, A.M.: “Statistical Fluid Mechanics: Mechanics of Turbulence”,
1011 vol. **2**, MIT Press. 1975
- 1012 Morrison, H., and W. W. Grabowski: Modeling supersaturation and subgrid-scale mixing
1013 with two-moment bulk warm microphysics. *J. Atmos. Sci.*, **65**, 792–812, 2008.
- 1014 Pinsky, M. and A. P. Khain: Effects of in-cloud nucleation and turbulence on droplet
1015 spectrum formation in cumulus clouds. *Quart. J. Roy. Meteorol. Soc.*, 128, 1–33, 2002.
- 1016 Pinsky M., I. P. Mazin, A. Korolev, and A. Khain: Supersaturation and diffusional droplet
1017 growth in liquid clouds. *J. Atmos. Sci.*, **70**, 2778-2793, 2013.
- 1018 Pinsky M., I. P. Mazin, A. Korolev and A. Khain: Supersaturation and diffusional droplet
1019 growth in liquid clouds: Polydisperse spectra. *J. Geophys. Res., Atmospheres*, **119**, 12,872–
1020 12,887, 2014.
- 1021 Pinsky, M., Khain, A., Korolev, A., and Magaritz-Ronen, L.: Theoretical study of mixing in
1022 liquid clouds. Part 2: Homogeneous mixing. *Atmos. Chem. Phys.*, , 2016 (submitted)
- 1023 Polyinin A. D. and V. F. Zaitsev: Handbook of nonlinear partial differential equations.
1024 Chapman & Hall/CRC, 809 pp. , 2004
- 1025 Prabha V. T., S. Patade, G. Pandithurai, A. Khain, D. Axisa, P. Pradeep Kumar, R. S.
1026 Maheshkumar, J. R. Kulkarni, and B. N. Goswami: Spectral width of premonsoon and
1027 monsoon clouds over Indo-Gangetic valley during CAIPEEX, *J. Geop. Res.* **117**, D20205,
1028 doi:10.1029/2011JD016837 , 2012
- 1029 Pruppacher, H.R., Klett, J.D.. Microphysics of Clouds and Precipitation. 2nd edn. Oxford
1030 Press, 914 p. , 1997

1031 Rogers R. R. and Yau M. K: A Short Course in Cloud Physics, Pergamon press. 293pp. ,
1032 1989

1033 Schlüter M. H.: The effects of entrainment and mixing process on the droplet size
1034 distribution in cumuli. A thesis submitted to the faculty of The University of Utah in partial
1035 fulfillment of the requirements for the degree of Master of Science, Department of
1036 Meteorology, The University of Utah, 92 pp., 2006

1037 Su C.-W., S.K. Krueger, P.A. McMurry and P.H. Austin: Linear eddy modeling of droplet
1038 spectral evolution during entrainment and mixing in cumulus clouds. *Atmos. Res.*, **47-48**, 41-
1039 58, 1998.

1040 Telford, J.W., and S. K. Chai: A new aspect of condensation theory. *Pageoph*, **118**, 720-
1041 742 , 1980

1042 Warner, J.: The microstructure of cumulus cloud. Pt. I, General features of the droplet
1043 spectrum, *J. Atmos. Sci.*, **26**, 1049-1059, 1969.

1044 Warner, J.. The microstructure of cumulus cloud: Part 4: The effect on the droplet spectrum
1045 of mixing between cloud and environment. *J. Atmos. Sci.* **30**, 256–261, 1973.

1046

1047

1048

1049

1050

1051

1052

1053

1054

1055

1056

1057 **Table 1. Main parameters of the problem and their non-dimensional forms***

1058

Quantity	Symbol	Non-dimensional form	Range of normalized values
Time	t	$\tilde{t} = \frac{t}{\tau_0}$	$[0 \dots \infty]$
Distance	x	$\tilde{x} = \frac{x}{L}$	$[0 \dots 1]$
Square of drop radius	σ	$\tilde{\sigma} = \frac{\sigma}{r_0^2}$	$[0 \dots 1]$
Droplet concentration	N	$\tilde{N} = \frac{N}{N_1}$	$[0 \dots 1]$
Liquid water mixing ratio	q	$\tilde{q} = \frac{q}{q_1}$	$[0 \dots 1]$
Distribution of square of drop radius	$g(\sigma)$	$\tilde{g}(\tilde{\sigma}) = \frac{r_0^2}{N_1} g(\sigma)$	
Conservative function	Γ	$\tilde{\Gamma} = \frac{\Gamma}{A_2 q_1}$	$[-\infty \dots 1]$
Supersaturation	S	$\tilde{S} = \frac{S}{A_2 q_1}$	$[-\infty \dots 0]$
Relaxation time	τ_{pr}	$\tilde{\tau}_{pr} = \frac{\tau_{pr}}{\tau_0}$	$[1 \dots \infty]$
Damköhler number	Da	$Da = \frac{\tau_{mix}}{\tau_0} = \frac{L^2}{K \tau_0}$	$[0 \dots \infty]$
Potential evaporation parameter (PEP)	R	$R = \frac{S_2}{A_2 q_1}$	$[-\infty \dots 0]$

1059

1060 *All normalized values depend on the initially given values of L , N_1 , r_0 , A_2 , S_2 and K

1061

1062

1063 **Table 2.** Comparison of analysis based on the classic concepts of mixing and the results of
 1064 the present study
 1065

Classical concept	The present study
Only the final equilibrium state is typically analyzed; results of in-situ observations are interpreted assuming the equilibrium state.	The mixing period can last several minutes and more. The microphysical structure of the mixing volumes during this period can differ substantially from that at the final state
Types of mixing are separated into homogeneous and extremely inhomogeneous.	There are the wide ranges of Da and R values, at which mixing can be regarded as intermediate or inhomogeneous (but not extremely inhomogeneous).
Mixing can start as purely homogeneous	Any mixing starts with the inhomogeneous stage
Homogeneous mixing leads to a DSD shift to small droplet sizes	Homogeneous mixing does not always lead to the DSD shift to small droplet sizes (Pt. 2). The shift depends on the DSD shape.
Mixing can be analyzed within the framework of a monodisperse DSD	Mixing always leads to formation of polydisperse DSD
In the course of homogeneous mixing, droplet concentration remains constant	In the course of homogeneous mixing, droplet concentration does not always remain constant (Pt. 2)
Extremely inhomogeneous mixing does not change the DSD shape	Inhomogeneous mixing (including extremely inhomogeneous) leads to broadening of the DSD towards small sizes
In the course of inhomogeneous mixing, the	The effective radius varies only slightly (5-20

effective radius remains constant	%) in the initially cloud volume. The effective radius rapidly increases in the initially droplet-free volume, approaching the value of effective radius in the cloud volume. With increasing Da , the difference between the values of the effective radius in the initially cloud volume and that at the final state decreases in agreement with the classic concept.
-----------------------------------	---

1066

1067

1068

1069

1070

1071

1072

1073

1074

1075

1076

1077

1078

1079

1080

1081

1082

1083

1084

Tab. A. List of symbols

1085

("nd" means non-dimensional)

Symbol	Description	Units
A_2	$\frac{1}{q_v} + \frac{L_w^2}{c_p R_v T^2}$, coefficient	nd
a_0, a_n	the Fourier series coefficients	nd
C	the Richardson's law constant	nd
c_p	specific heat capacity of moist air at constant pressure	$\text{J kg}^{-1} \text{K}^{-1}$
\mathcal{D}	coefficient of water vapour diffusion in the air	$\text{m}^2 \text{s}^{-1}$
Da	the <i>Damköhler</i> number	nd
e	water vapor pressure	N m^{-2}
e_s	saturation vapour pressure above a flat water surface	N m^{-2}
F	$F = \frac{\rho_w L_w^2}{k_a R_v T^2} + \frac{\rho_w R_v T}{e_s(T) \mathcal{D}}$, coefficient	$\text{m}^{-2} \text{s}$
$f(r)$	droplet size distribution	m^{-4}
$g(\sigma)$	distribution of square radius	m^{-5}
$\tilde{g}(\tilde{\sigma})$	normalized distribution of square radius	nd
k_a	coefficient of air heat conductivity	$\text{J m}^{-1} \text{s}^{-1} \text{K}^{-1}$
K	turbulent diffusion coefficient	$\text{m}^2 \text{s}^{-1}$
L	characteristic spatial scale of mixing	m
L_w	latent heat for liquid water	J kg^{-1}
m_α	moment of DSD of order α	m^{-3}
N	droplet concentration	
\tilde{N}	normalized droplet concentration	nd
N_1	Initial droplet concentration in a cloud volume	m^{-3}
p	pressure of moist air	N m^{-2}
q	liquid water mixing ratio	kg/kg
q_1	Initial liquid water mixing ratio in a cloudy volume	kg/kg
q_v	water vapor mixing ratio	kg/kg
\tilde{q}	normalised liquid water mixing ratio equal to	nd

	normalized LWC	
r	droplet radius	m
r_0	initial droplet radius	m
r_0	mean droplet radius	m
r_v	mean volume radius	m
R	$\frac{S_2}{A_2 q_1}$, potential evaporation parameter (PEP)	nd
R_a	specific gas constant of moist air	$\text{J kg}^{-1} \text{K}^{-1}$
R_v	specific gas constant of water vapor	$\text{J kg}^{-1} \text{K}^{-1}$
S	$e/e_w - 1$, supersaturation over water	nd
\tilde{S}	normalized supersaturation	nd
S_2	Initial supersaturation in a dry volume	nd
\tilde{S}_{\max}	maximal normalized supersaturation	nd
T	temperature	K
T_{mix}	normalized duration of inhomogeneous stage	nd
T_{ev}	normalized duration of evaporation	nd
T_{tot}	normalized duration of mixing	nd
t	time	s
\tilde{t}	non-dimensional time	nd
x	distance	m
\tilde{x}	non-dimensional distance	nd
λ_1, λ_2	criteria of delimitation between the types of mixing	nd
ε	turbulent dissipation rate	$\text{m}^2 \text{s}^{-3}$
$\Gamma(x, t)$	conservative function	nd
$\tilde{\Gamma}$	normalized conservative function	nd
ρ_a	air density	kg m^{-3}
ρ_w	density of liquid water	kg m^{-3}
σ	square of droplet radius	m^2
$\tilde{\sigma}$	normalized square of droplet radius	nd
τ_{pr}	phase relaxation time	s

$\tilde{\tau}_{pr}$	normalized phase relaxation time	nd
τ_{mix}	characteristic time of mixing	s
τ_0	Initial time scale	s

1086

1087

1088

1089

1090

1091

1092

1093

1094

1095

1096

1097

1098

1099

1100

1101

1102

1103

1104

1105

1106

1107

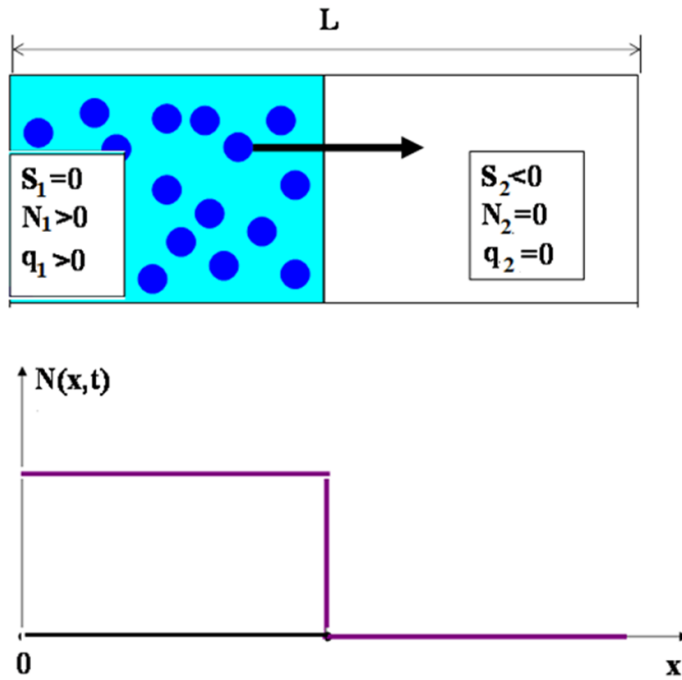
1108

1109 **Figures**

1110

1111

1112



1113

1114

1115 **Fig.1.** The schematic illustration of the 1D mixing problem considered in the study. The

1116 initial state at $t = 0$ is illustrated. The left volume of length $L/2$ is a saturated cloudy volume;

1117 the right volume is a non-saturated air volume from the cloud environment.

1118

1119

1120

1121

1122

1123

1124

1125

1126

1127

1128

1129

1130

1131

1132

1133

1134

1135

1136

1137

1138

1139

1140

Fig. 2. An example of $\Gamma(x,t)$ evolution during mixing.

1141

1142

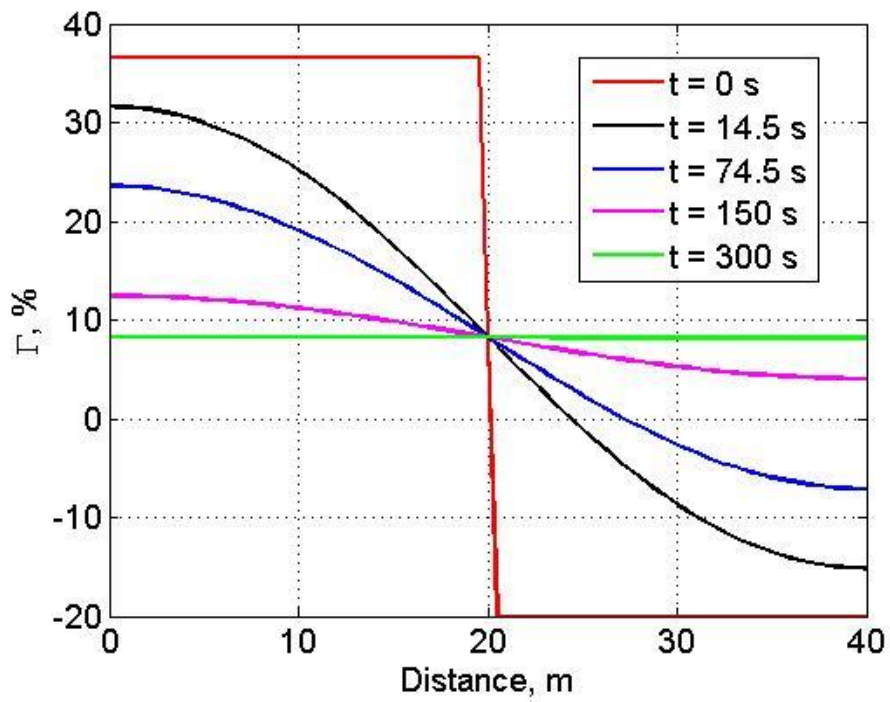
1143

1144

1145

1146

1147



1148

1149

1150

1151

1152

1153

1154

1155

1156

1157

1158

1159

1160

1161

1162

1163

1164

1165

1166

1167

1168

1169

1170

1171

1172

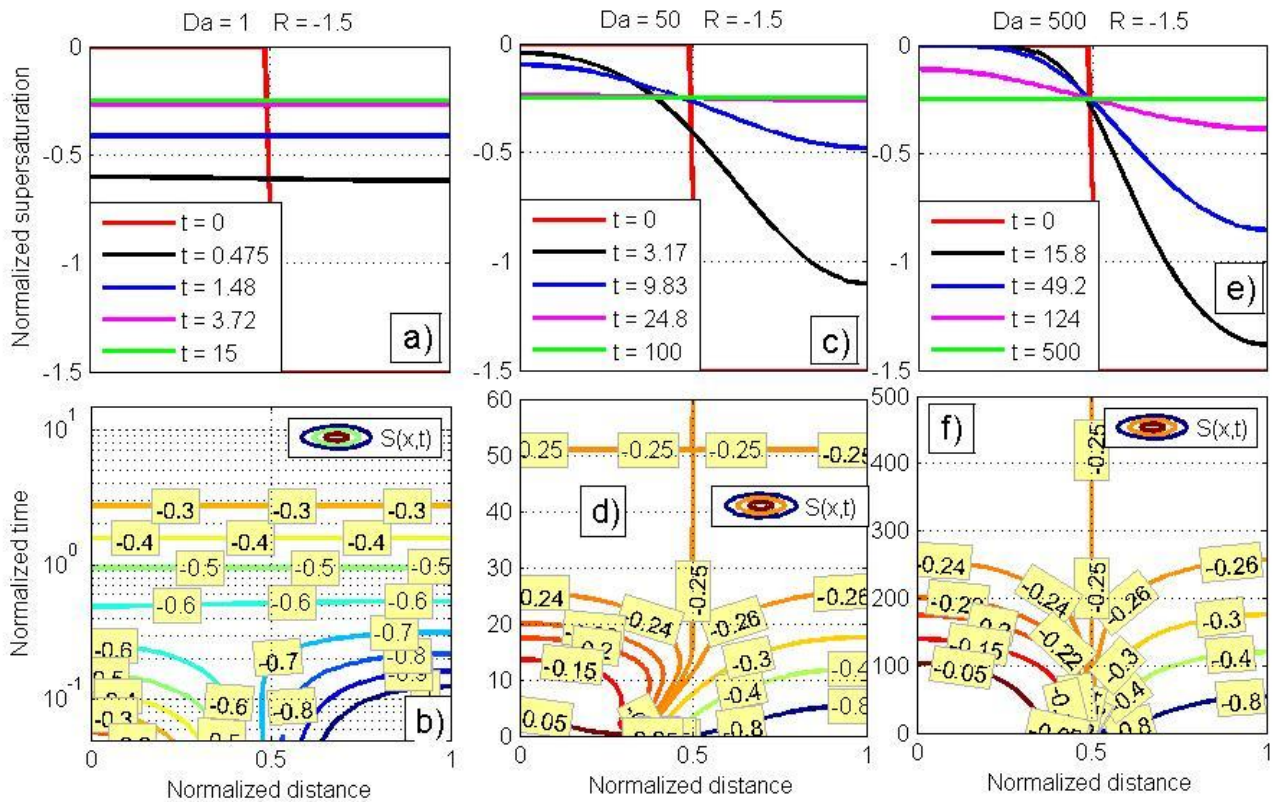


Fig. 3. Horizontal dependencies (upper row) and $\tilde{x}-\tilde{t}$ dependencies (lower row) of normalized supersaturation at $Da = 1$, $Da = 50$ and $Da = 500$ and at $R = -1.5$. Panel b is plotted in semi-log scale.

1173

1174

1175

1176

1177

1178

1179

1180

1181

1182

1183

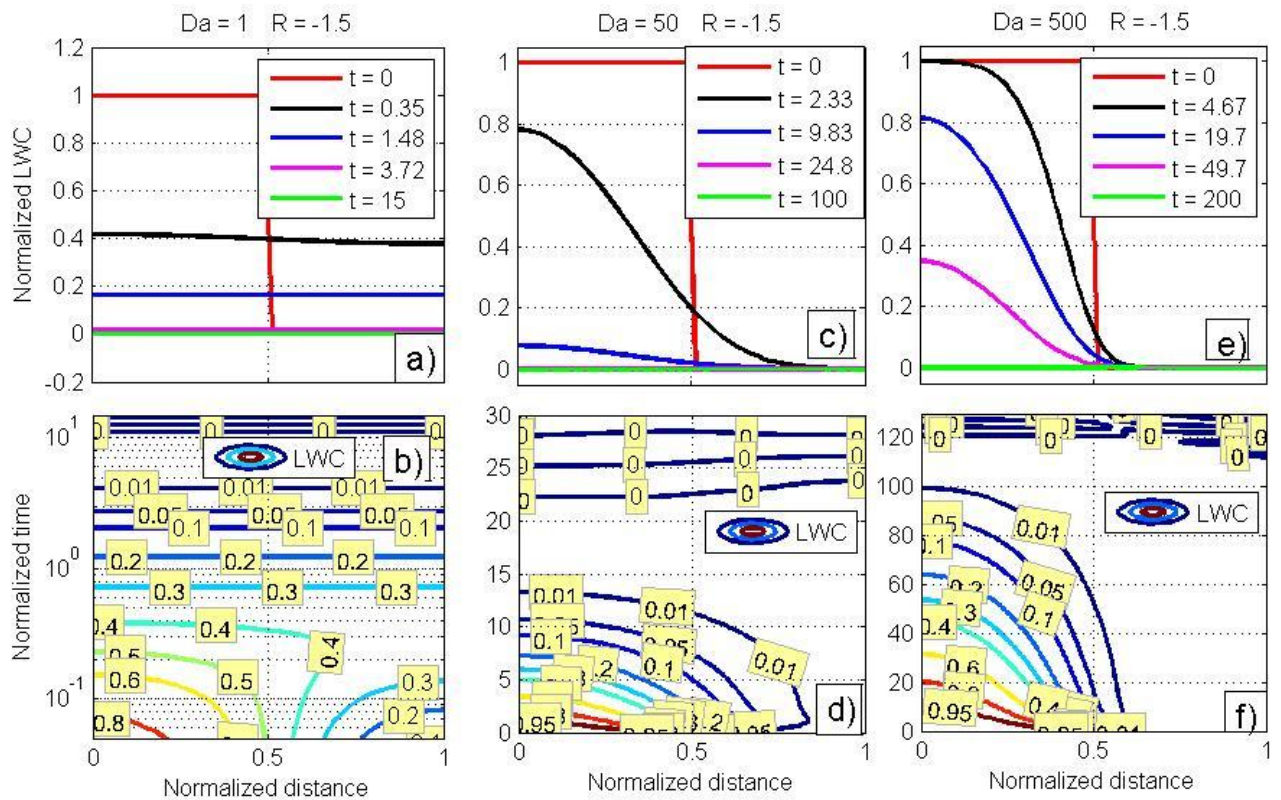
1184 **Fig. 4.** The same as in Fig. 3, but for normalized LWC. Left bottom panel is plotted in
 1185 semi-log scale.

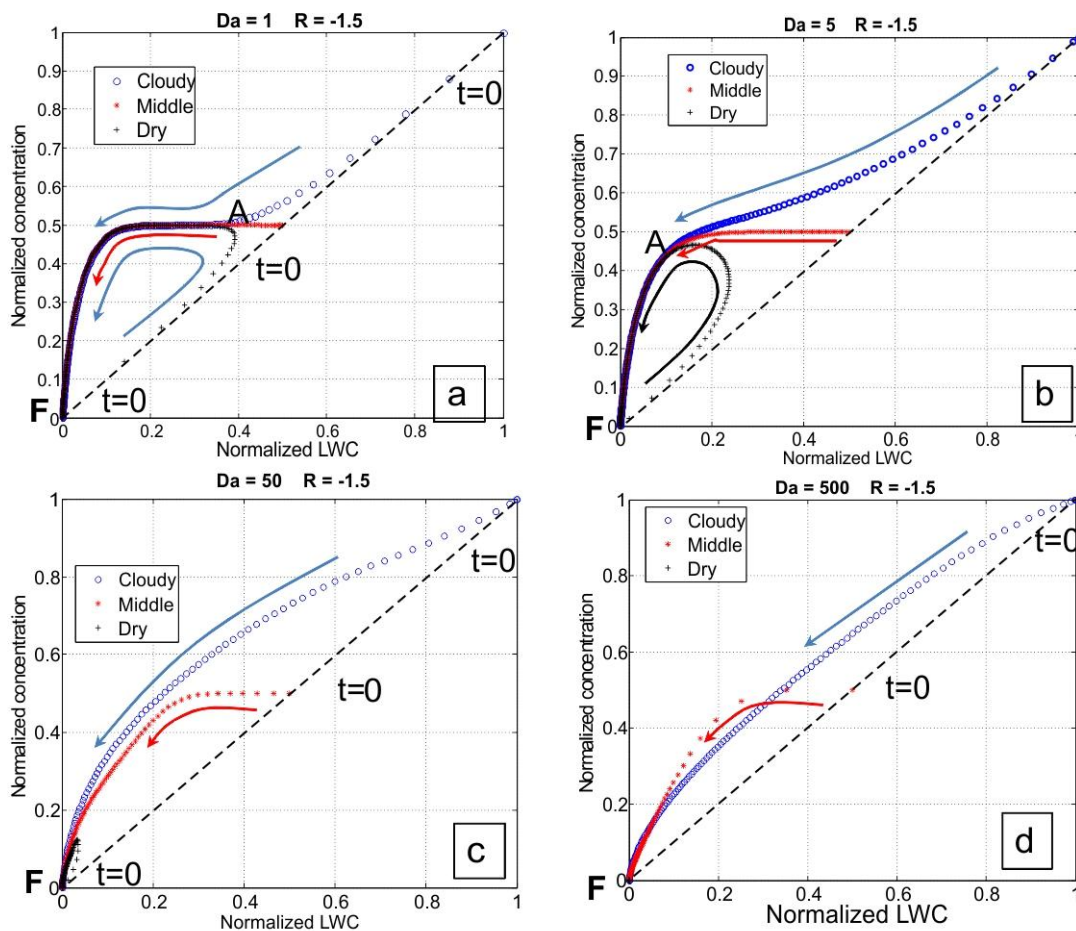
1186

1187

1188

1189





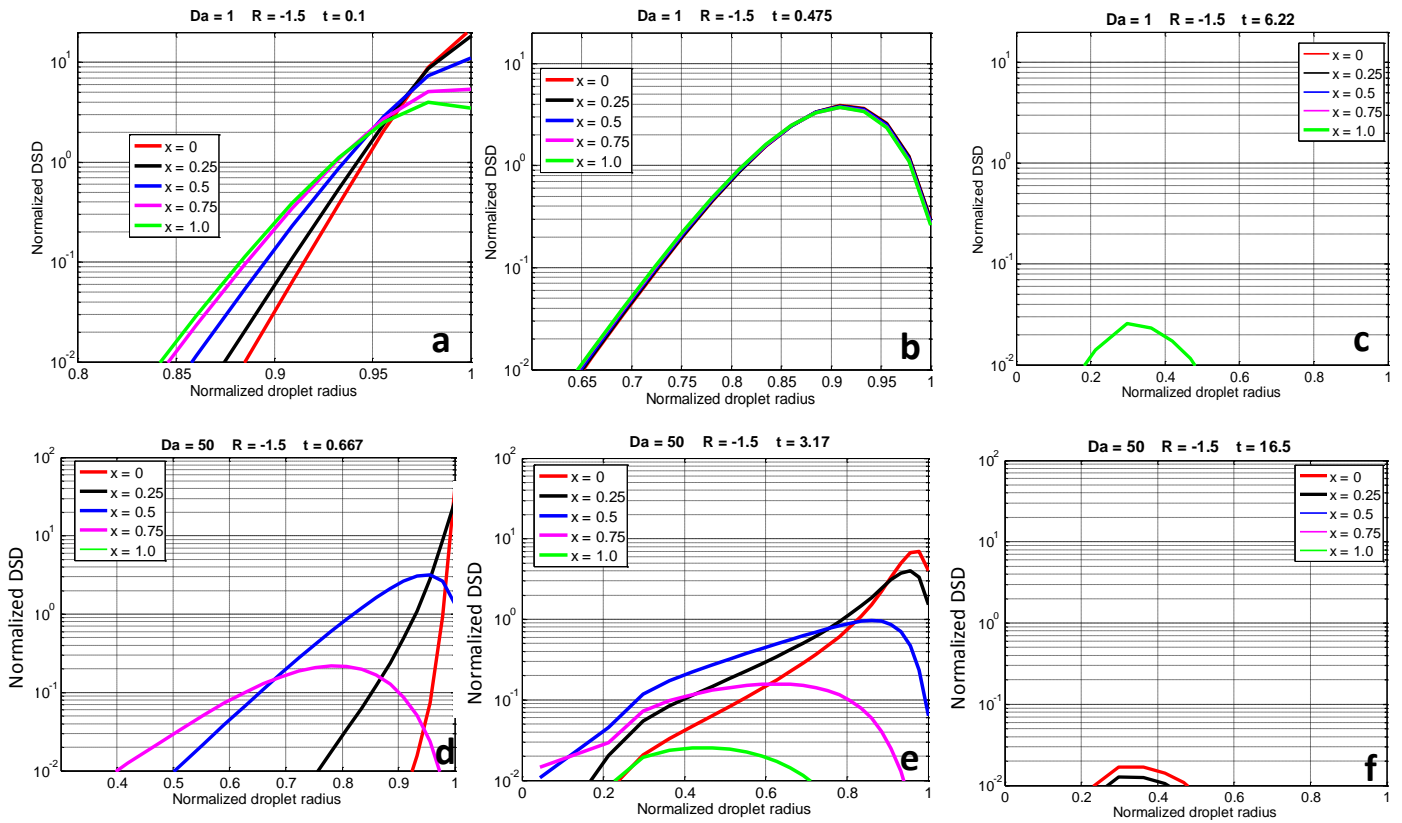
1190

1191 **Fig. 5.** Dependencies of normalized values of droplet concentration on normalized LWC
 1192 at different Da and $R = -1.5$. Blue symbols mark the centre of the cloudy volume ($\tilde{x} = 1/4$),
 1193 red symbols mark the interface between the cloudy volume and the dry volume ($\tilde{x} = 1/2$), and
 1194 black crosses mark the centre of the initially droplet-free volume ($\tilde{x} = 3/4$). Symbols are
 1195 plotted at different time instances. Symbols at $t=0$ show initial values of droplet concentration
 1196 and LWC at the three values of \tilde{x} . Arrows show the direction of movement of the points at the
 1197 diagram with time. Point “A” marks the beginning of the spatially homogeneous stage, $\tilde{t} = T_{mix}$.
 1198 Point “F” marks the final state. The dashed line indicates the relationship between \tilde{N} and \tilde{q} in
 1199 extremely inhomogeneous mixing (according to the classical concept).

1200

1201

1202



1203

1204

1205 **Fig. 6** Time evolution of DSD during droplet evaporation at $Da=1$ (upper row) and
 1206 $Da = 50$ (bottom row). In each panel, the normalized DSD are shown at different values of
 1207 horizontal coordinate \tilde{x} . Different panels show DSD at different time instances.

1208

1209

1210

1211

1212

1213

1214

1215

1216

1217

1218

1219

1220

1221

1222

1223

1224

1225

1226

1227

1228

1229

1230

1231

1232

1233

1234

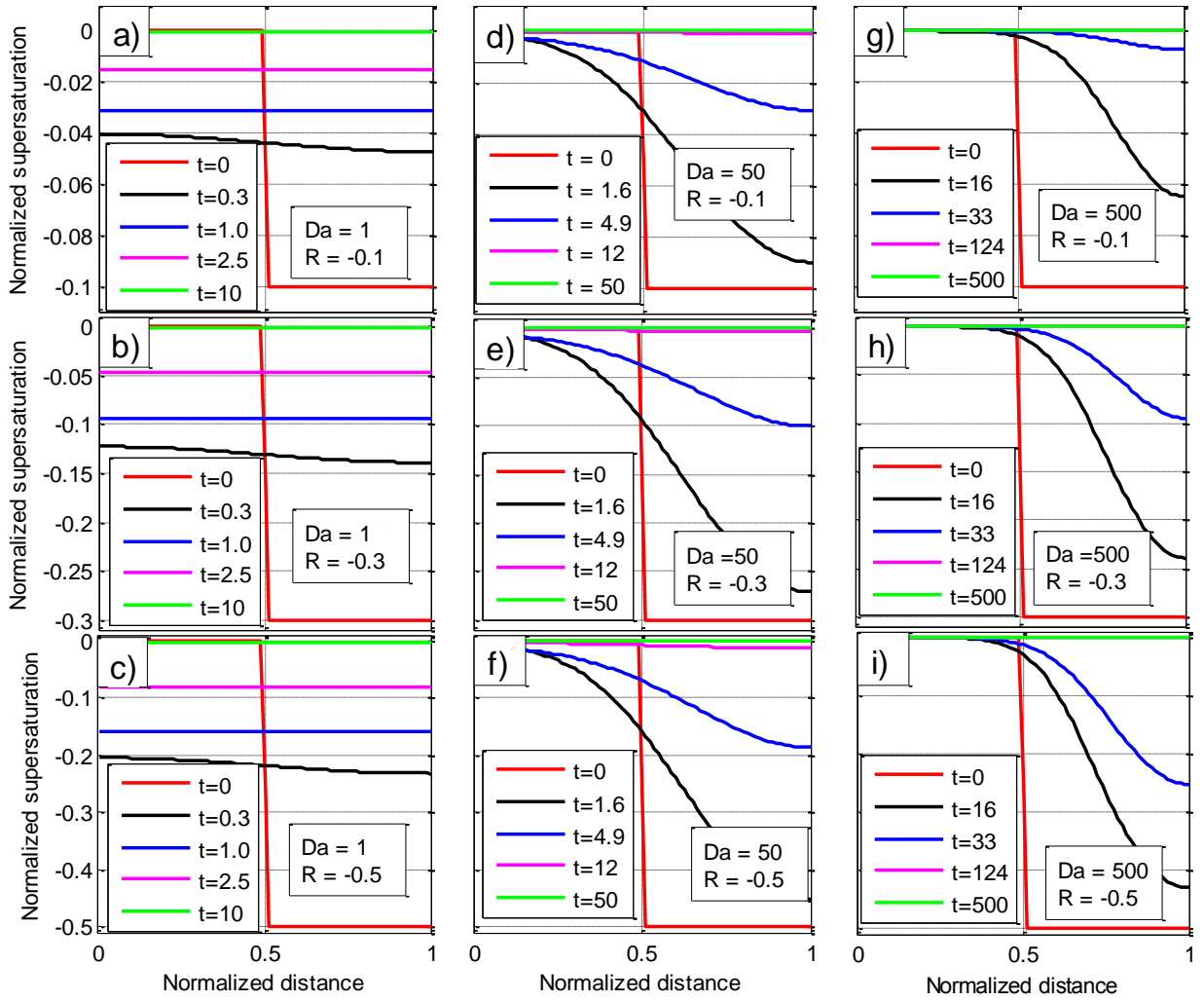


Fig. 7. Profiles of normalized supersaturation at different Da and different $R > -1$.

1235

1236

1237

1238

1239

1240

1241

1242

1243

1244

1245

1246

1247

1248

1249

1250 **Fig. 8.** Profiles of normalized LWC at different Da and at different $R > -1$.

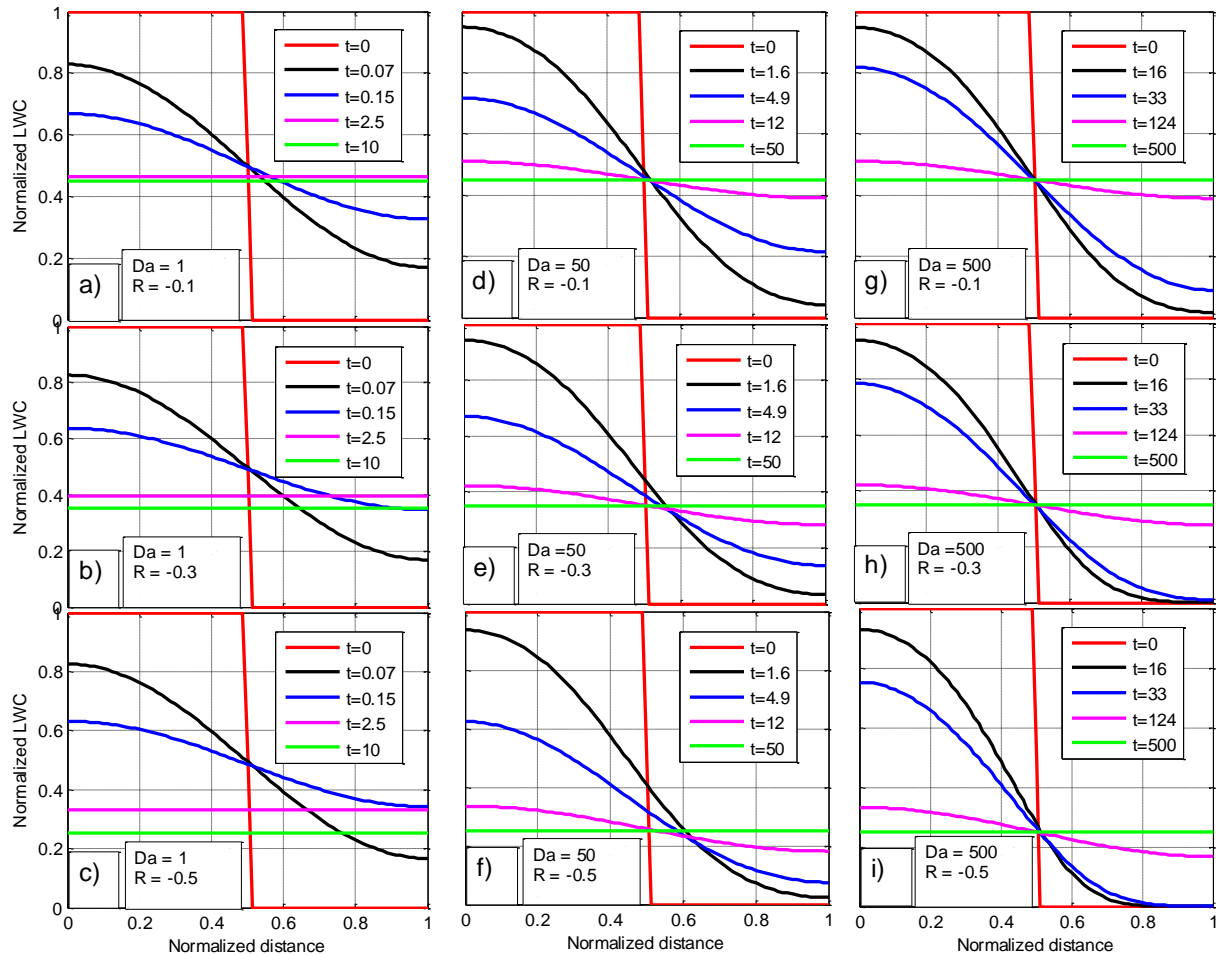
1251

1252

1253

1254

1255



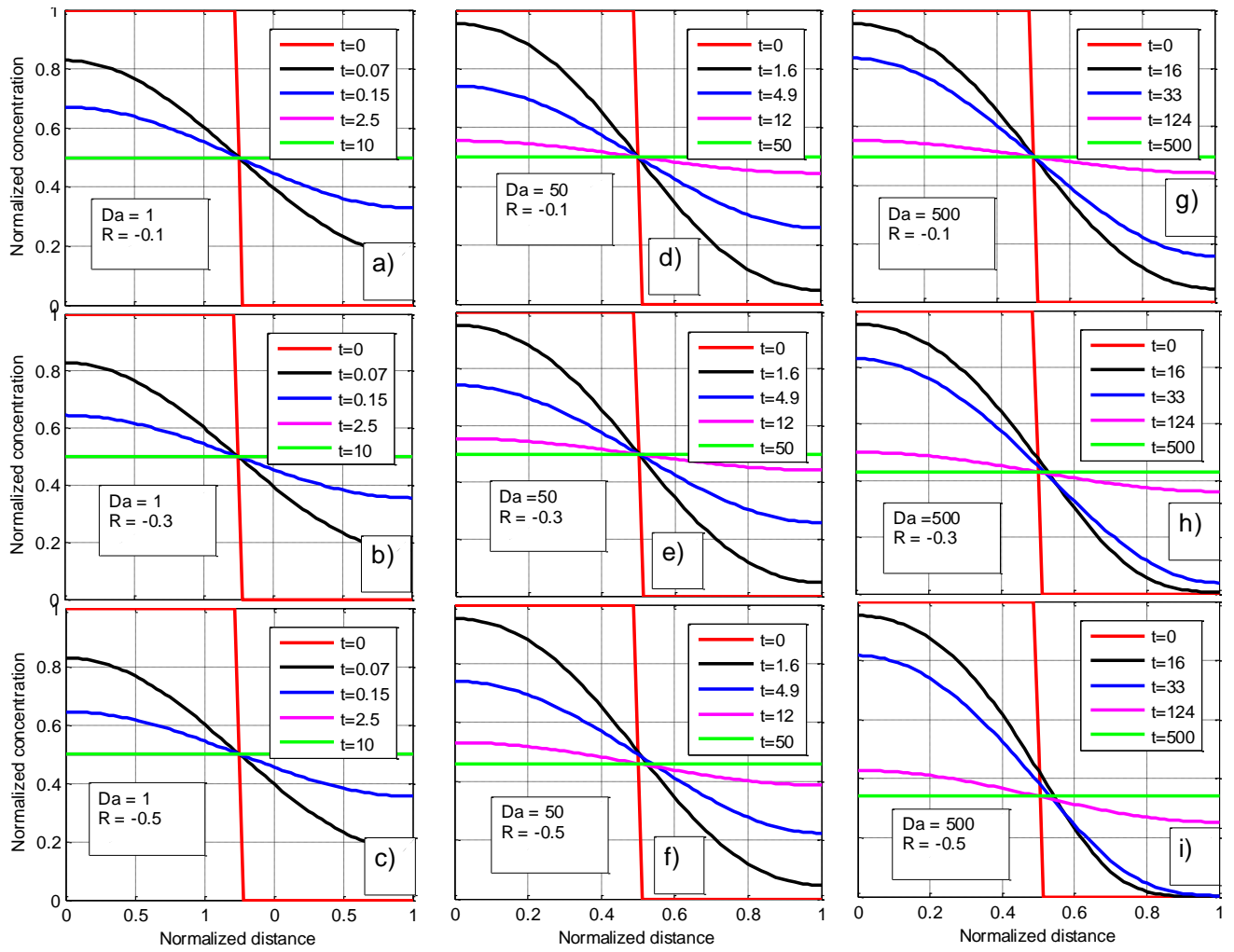
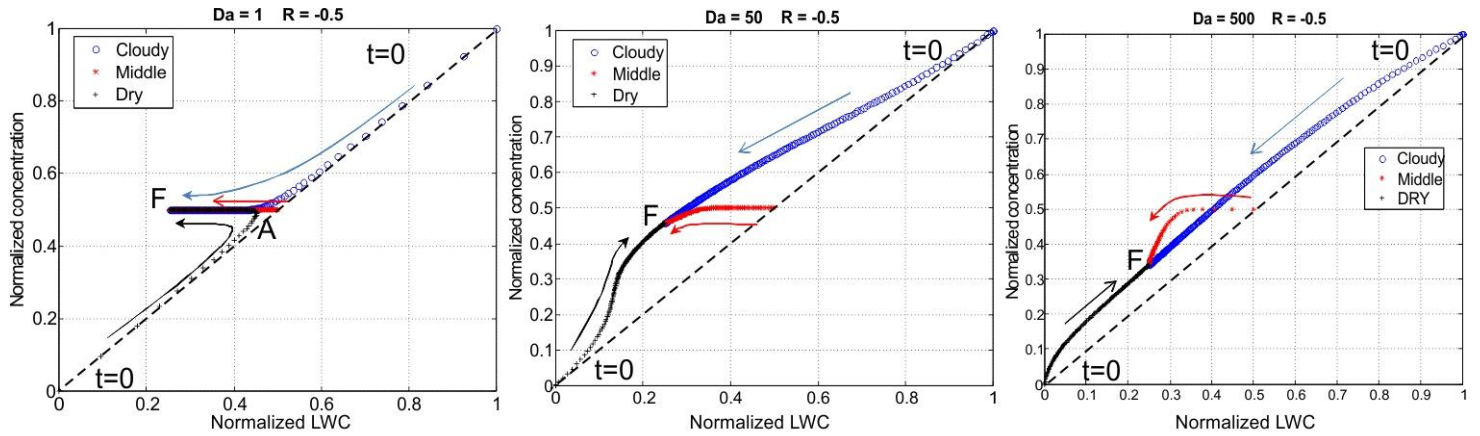


Fig. 9. Profiles of normalized droplet concentration at different Da and at different $R > -1$.

1281

1282



1283

1284

1285 **Fig. 10.** Dependencies of normalized values of droplet concentration on normalized LWC
 1286 at different Da and at $R = -0.5$. Blue circles mark the centre of the cloudy volume ($\tilde{x} = 1/4$),
 1287 red symbols mark the initial interface ($\tilde{x} = 1/2$) and black crosses mark the centre of the
 1288 initially dry volume ($\tilde{x} = 3/4$). Arrows show the direction of movement of the points with
 1289 time. Point “F” marks the final stationary state of the system. The dashed line indicates the
 1290 relationship between \tilde{N} and \tilde{q} in extremely inhomogeneous mixing (according to the classical
 1291 concept).

1292

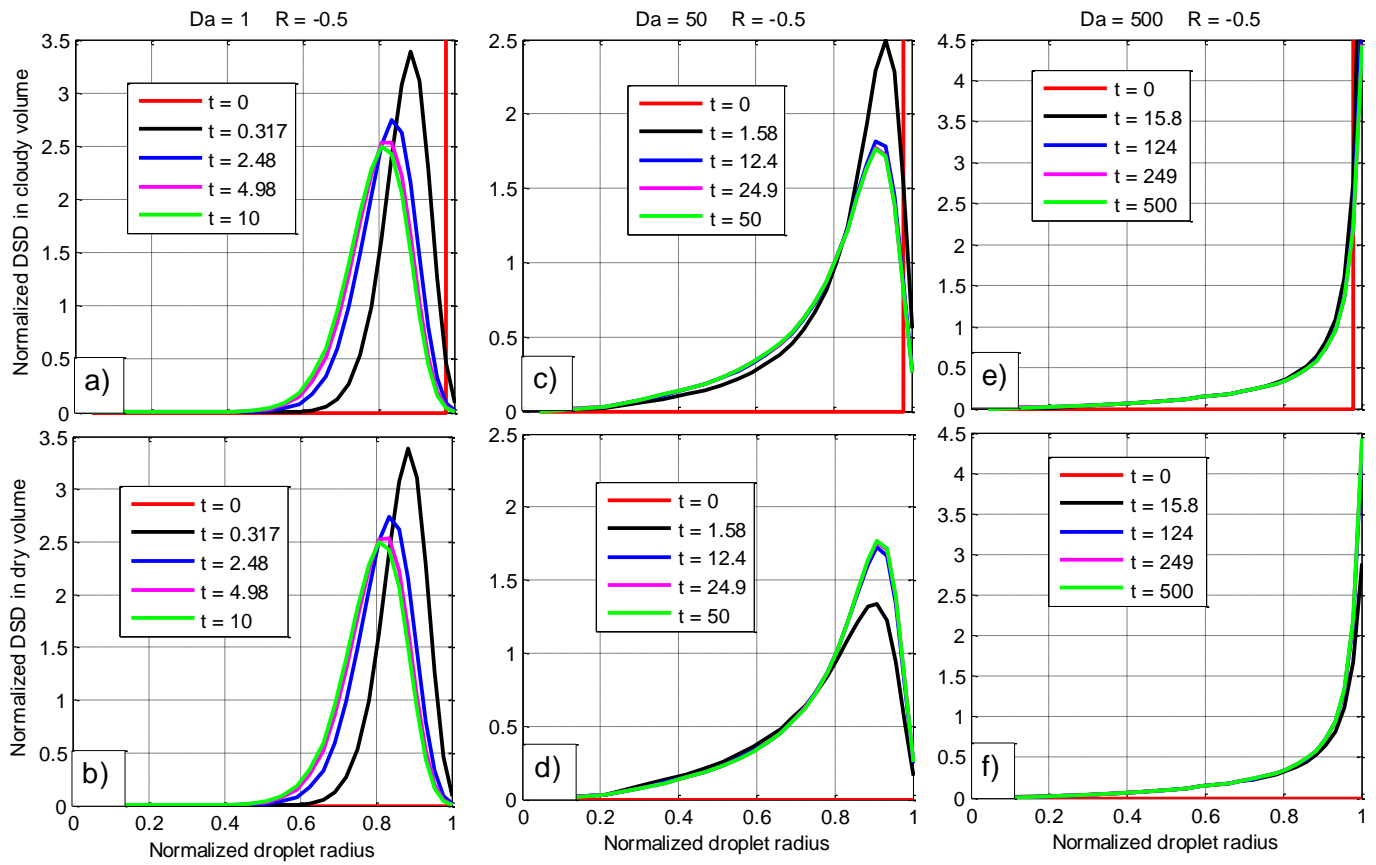
1293

1294

1295

1296

1297



1298

1299

1300

1301 **Fig. 11** Examples of DSD evolution in the initially cloudy volume ($\tilde{x} = 1/4$) (upper row)

1302 and in the initially dry volume ($\tilde{x} = 3/4$) (lower row) at $R = -0.5$ and at different values of

1303 Da .

1304

1305

1306

1307

1308

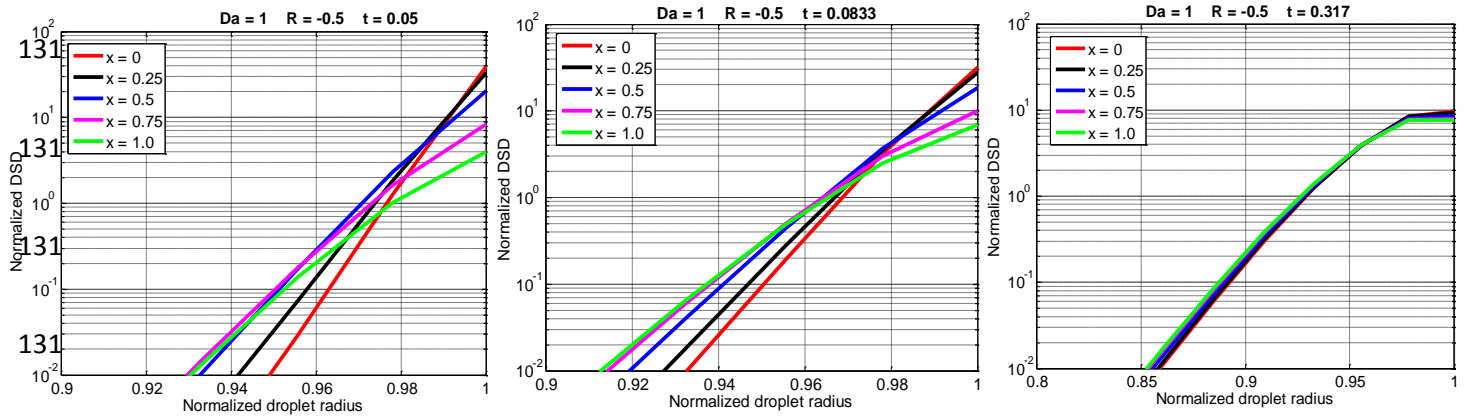
1309

1310

1311

1312

1313



1318

1319

1320

1321

1322 **Fig. 12.** DSD at different \tilde{x} at the beginning of the mixing process for $Da=1$ and1323 $R = -0.5$.

1324

1325

1326

1327

1328

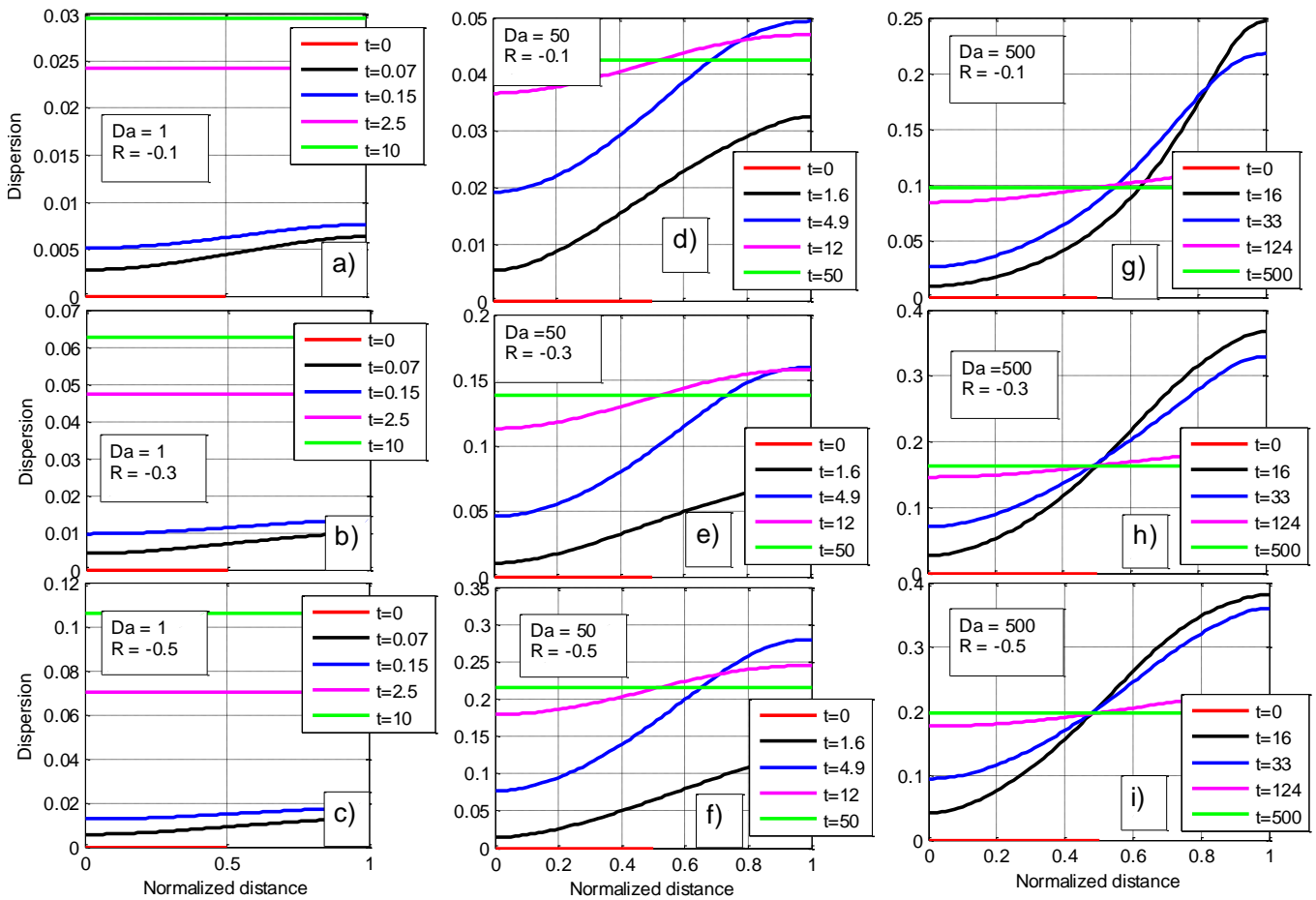
1329

1330

1331

1332

1333



1334

1335

1336 **Fig. 13.** Spatial dependencies of the relative DSD dispersion at different time instances and1337 at different values of Da and different $R > -1$

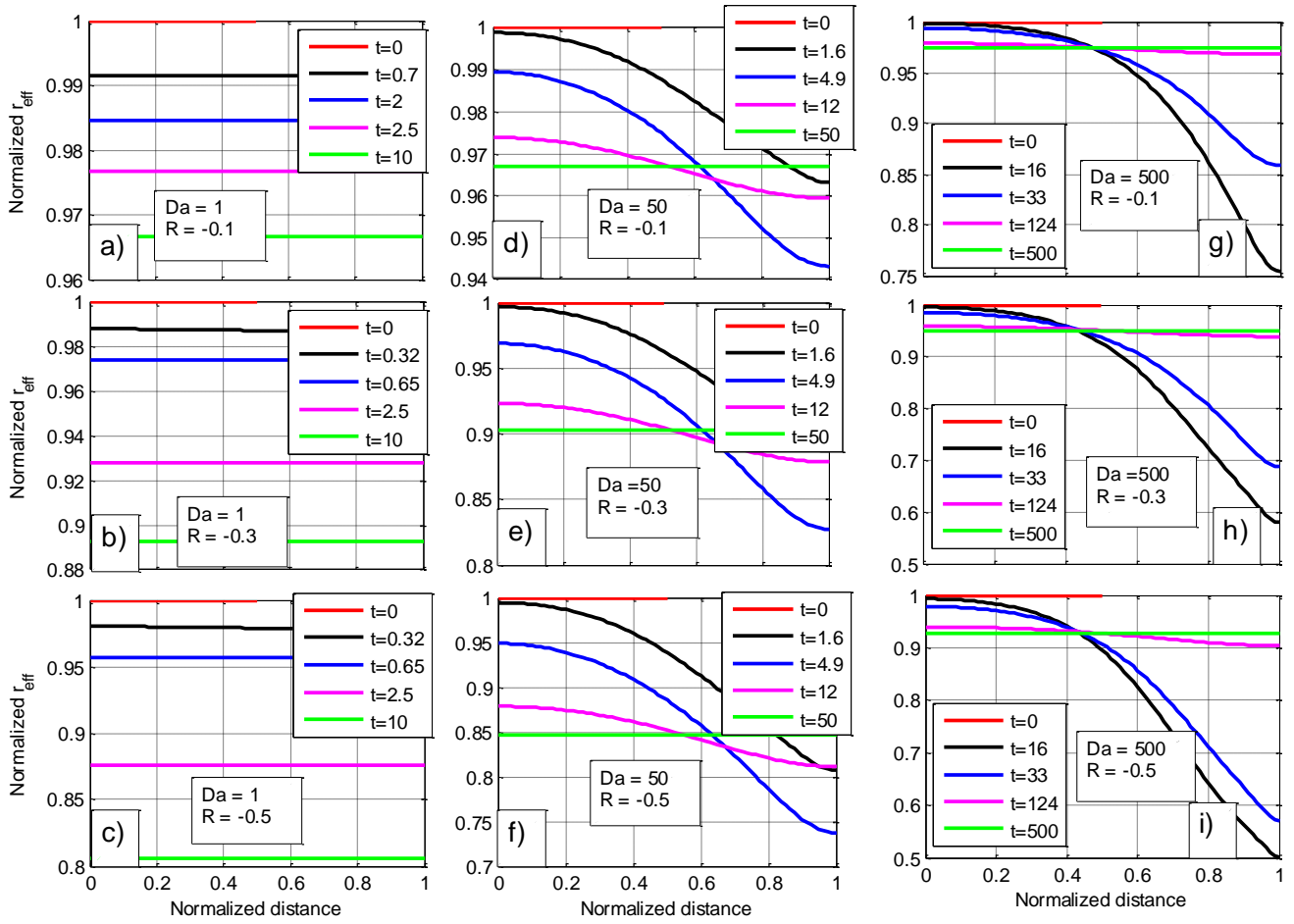
1338

1339

1340

1341

1342



1343

1344

1345 **Fig. 14.** Spatial dependencies of the effective radius at different time instances and at
 1346 different values of Da and different $R > -1$

1347

1348

1349

1350

1351

1352

1353

1354

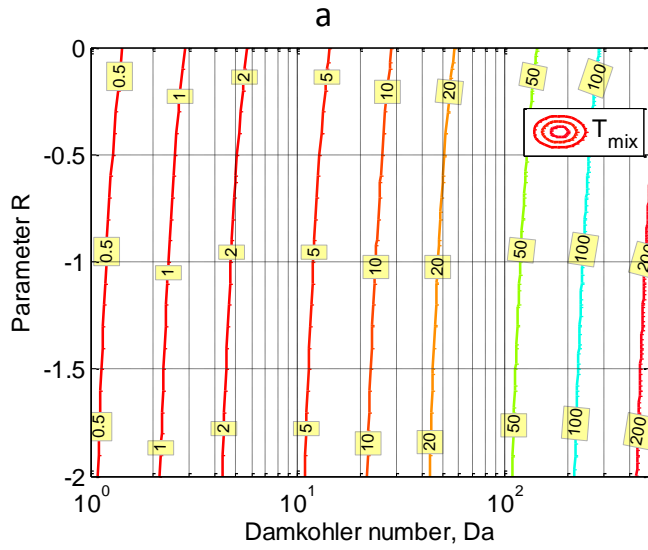
1355

1356

1357

1358

1359



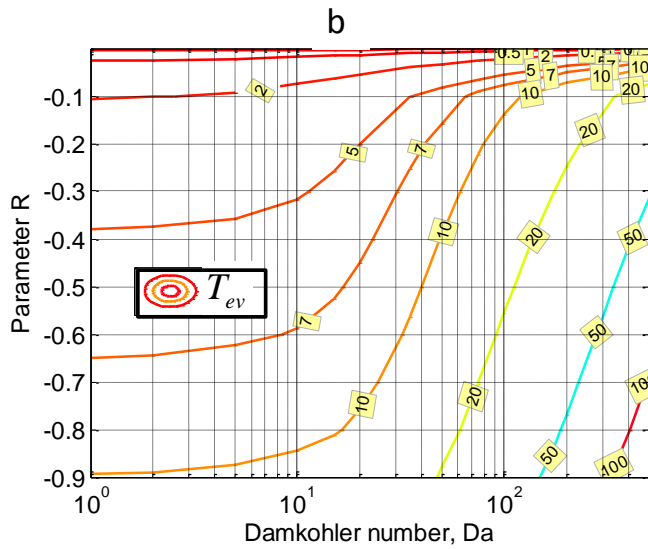
1360

1361

1362

1363

1364



1365

1366

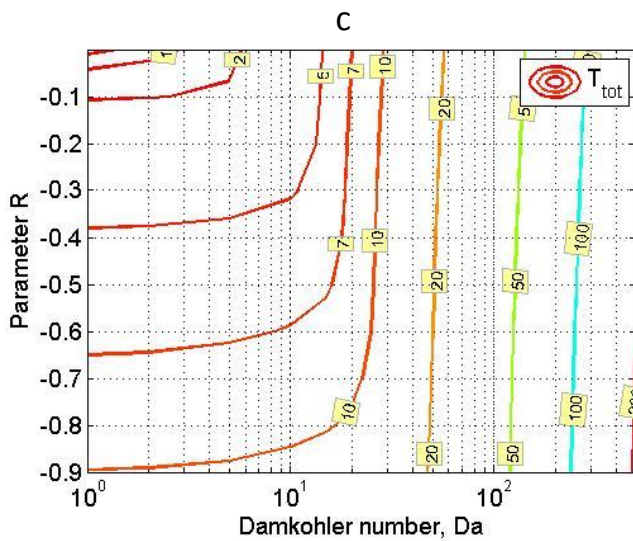
1367

1368

1369

1370

1371

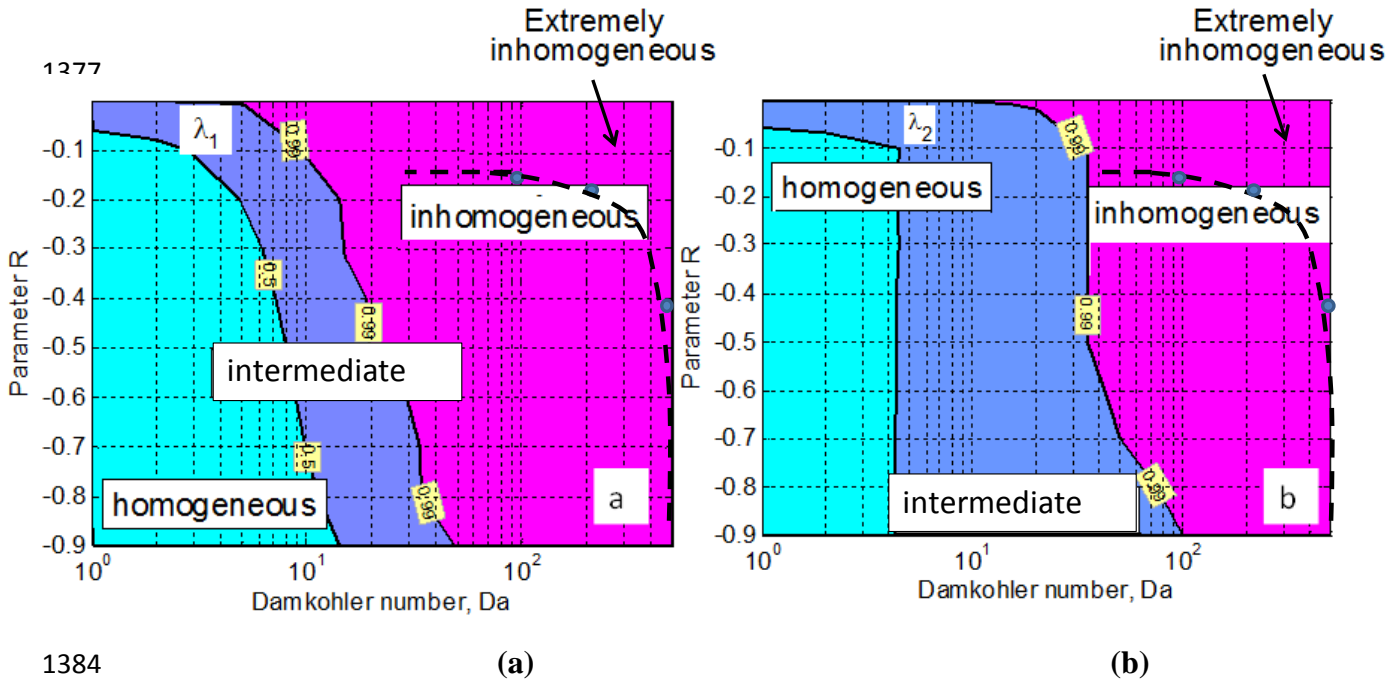


1372 **Fig. 15.** Contours of normalized mixing duration times on $Da-R$ plane. (a) mixing time
 1373 T_{mix} , (b) evaporation time T_{ev} , and (c) the total duration mixing time T_{tot} .

1374

1375

1376



1385

1386 **Fig. 16.** (a) The boundaries between mixing types on the $Da-R$ plane designed according

1387 to criteria $\lambda_1 = \frac{T_{mix}}{T_{tot}}$; (b) The boundaries between mixing types on the $Da-R$ plane designed

1388 according to criterion $\lambda_2 = \frac{2\langle \tilde{q}(T_{mix}) \rangle - 1}{R}$ (Eq. 41). Dashed lines indicate the line corresponding

1389 to 2% deviation from the initial mean volume radius.

1390

1391

1392

1393

1394

1395

1396

1397

1398

1399

1400

1401

1402

1403

1404

1405

1406

1407

1408

1409

1410

1411

1412

1413

1414

1415

1416

1417

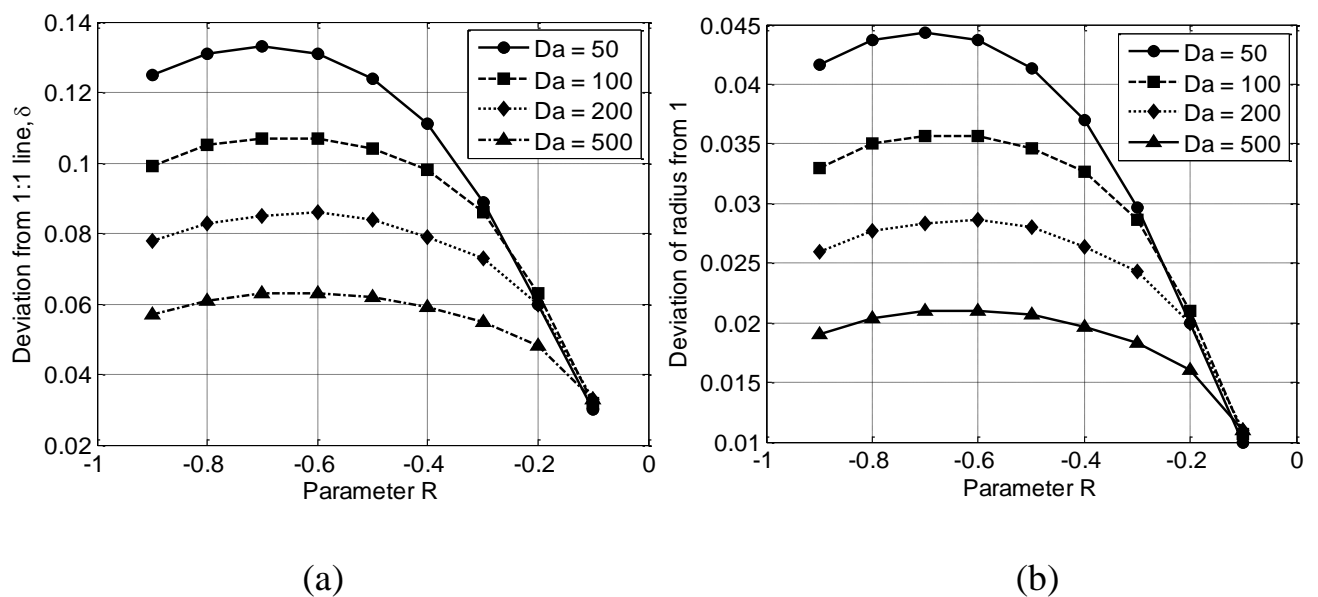


Fig 17. (a) Dependencies of the r.m.s. distance of the $\tilde{N} - \tilde{q}$ relationship curve from straight line 1:1 suggested by classical concept of extremely inhomogeneous mixing. The dependencies are plotted for different values of Da and R . (b) The same as to the left panel but for r.m.s. deviations of the mean volume radius curve from that initial constant value assumed in the classical concept.